CHAPTER SIX

EIS Studies on the Nano-Composite Polymer Electrolytes (NCPEs)

6.1 Introduction

The main aim of this chapter is to study the effect of alumina (Al_2O_3) nanoparticle on electrical and dielectric properties of CS:AgTf, CS:NaTf and CS:LiTf solid polymer electrolytes. Polymer–inorganic filler composite materials have been extensively studied for along time; these are called nano-composites if they employ nano-sized inorganic filler. They combine the advantages of the inorganic material (e.g., rigidity and thermal stability) and organic polymer (e.g., flexibility, dielectric and processability) [Tripathi and Shahi, 2011]. Till now, the nanoparticles most used are TiO_2, Al_2O_3, SiO_2, MgO etc. Adding these nanoparticles to SPE is found to be one of the most effective routes of achieving balanced characteristics of ionic conductivity and mechanical stability [Borgohain et al., 2010]. Thus the main objective of this chapter is to demonstrate the role of Al_2O_3 nanoparticles on DC conductivity and dielectric constant enhancement and their correlation in NCPE. The study of the Arrhenius and compensated Arrhenius behaviors, relaxation process, impedance and AC plots in NCPEs will also be investigated.

6.2 Electrical/Dielectric properties of NCPEs based on $(1-x)(0.9CS:0.1AgTf)$-xAl_2O_3 $(0.02 \leq x \leq 0.1)$

6.2.1 DC conductivity and Dielectric analysis of NCPE based on $(1-x)(0.9CS:0.1AgTf)$-xAl_2O_3 $(0.02 \leq x \leq 0.1)$

Figure 6.1 shows the DC conductivity variation of CS:AgTf(CSA6) with various concentrations of Al_2O_3 nanoparticles. It can be seen that the DC conductivity increased on addition of 2 to 4 wt.% Al_2O_3 nanoparticle and thereafter decreased with further addition of alumina nanoparticles. Compared to CS:AgTf (CSA6) system the DC conductivity of $(1-x)(0.9CS:0.1AgTf)$-xAl_2O_3 $(0.02 \leq x \leq 0.1)$ compositions is one order increased. The DC conductivity enhancement can be ascribed to the high dielectric constant of Al_2O_3 (8-10) [Li et al., 2007], which is more than the dielectric constant of pure chitosan and thus can dissociate more ions.
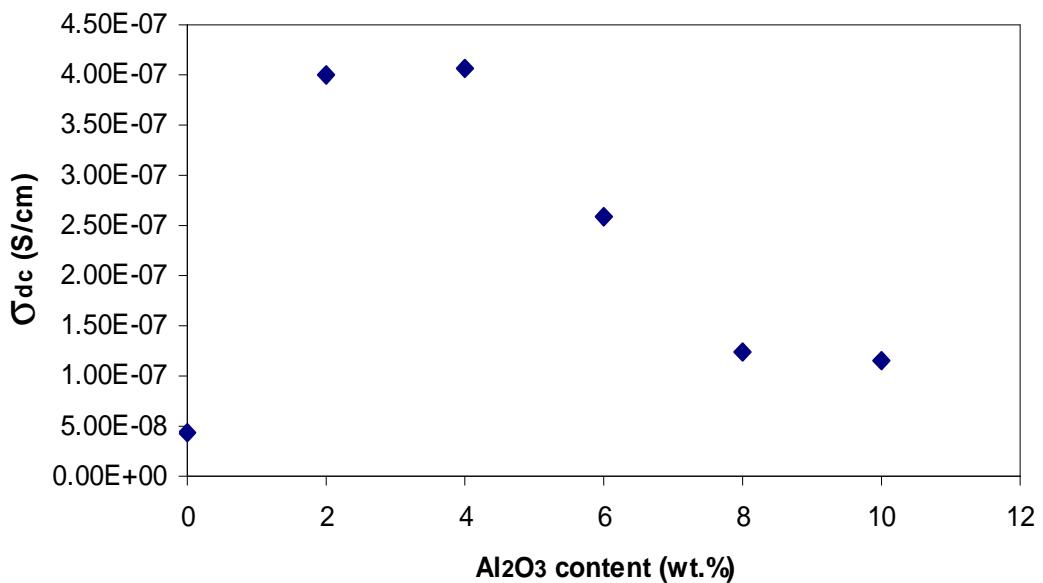
Figure 6.1: The ionic conductivity of chitosan:AgTf (CSA6) with various concentration of Al_2O_3.

Figure 6.2 shows the variation of DC conductivity with temperature for different concentrations of alumina filler. It is clear that the DC conductivity of all the NCPE compositions decreased at a particular temperature which may be related to the phase transition of alumina nanoparticles. The calculated actvation energy E_a for the CSNA2 highest conducting sample is 0.998 eV with the regression value $R^2=0.98$ in the low temperature (before drop in conductivity).
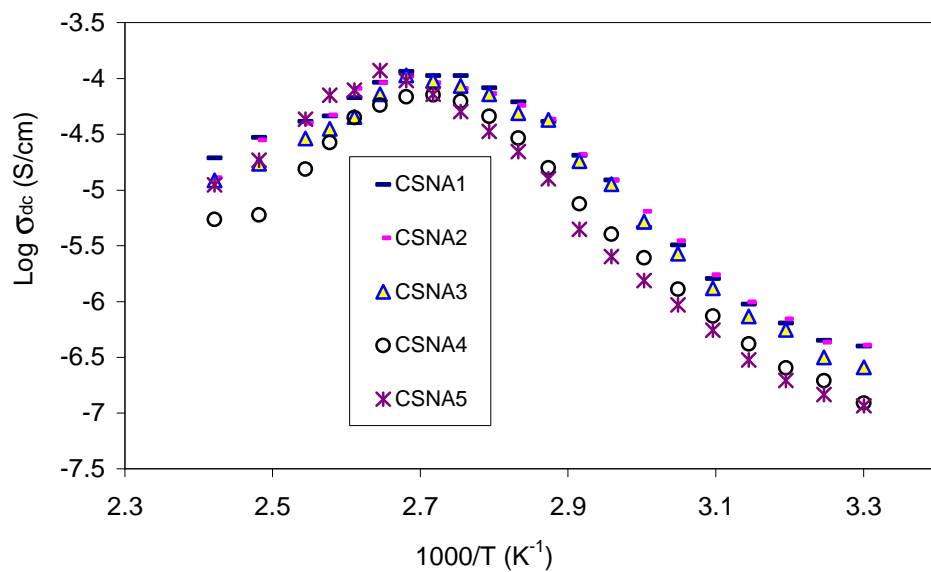
Figure 6.2 Temperature dependence of ionic conductivity of (1-x)(0.9CS:0.1AgTf)-xAl$_2$O$_3$ (0.02 ≤ x ≤ 0.1) nano-composite system.

In the previous chapter, the role of dielectric constant on conductivity behavior of solid polymer electrolytes has been illustrated. It is well known that clays and ceramic filler have high dielectric constant which is responsible for the conductivity enhancement of polymer electrolytes as a result of more salt dissociation [Deka and Kumar, 2010]. Figure 6.3 shows the frequency dependence of dielectric constant at room temperature for different concentrations of alumina filler. Due to the high electrode polarization the dielectric constant in the high frequency region for all compositions almost collapsed to

a single curve. By separation of the electrode part from the bulk part (high frequency) one can understand that the bulk material also exhibits a response to the presence of filler.
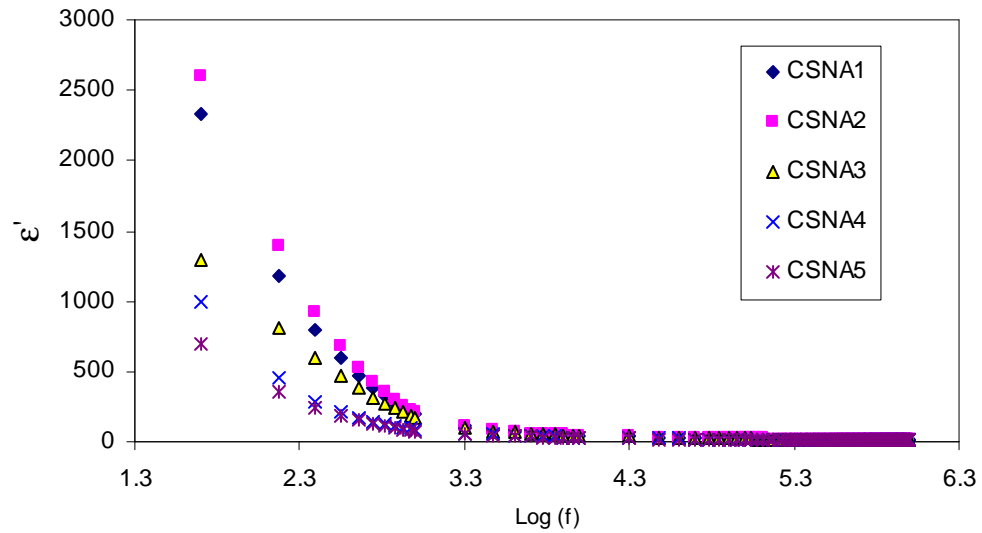
Figure 6.3 Composition dependence of dielectric constant for (1-x)(0.9CS:0.1AgTf)-xAl$_2$O$_3$ (0.02 ≤ x ≤ 0.1) NCPEs.

Figure 6.4 shows the bulk dielectric (high frequency) constant for different concentrations of alumina. It is clear that the bulk dielectric constant is almost frequency independent and increased with increasing filler content until 4 wt.% and thereafter decreased with increasing filler concentration as occurred for DC conductivity.

These results indicate the fact that DC conductivity is strongly dielectric constant dependent as observed this phenomenon also for solid polymer electrolytes based on CS:AgTf. Thus the increase of DC conductivity of NCPES based on CSNAs compared to solid polymer electrolytes based on CS:AgTf is due to the dielectric constant enhancement.
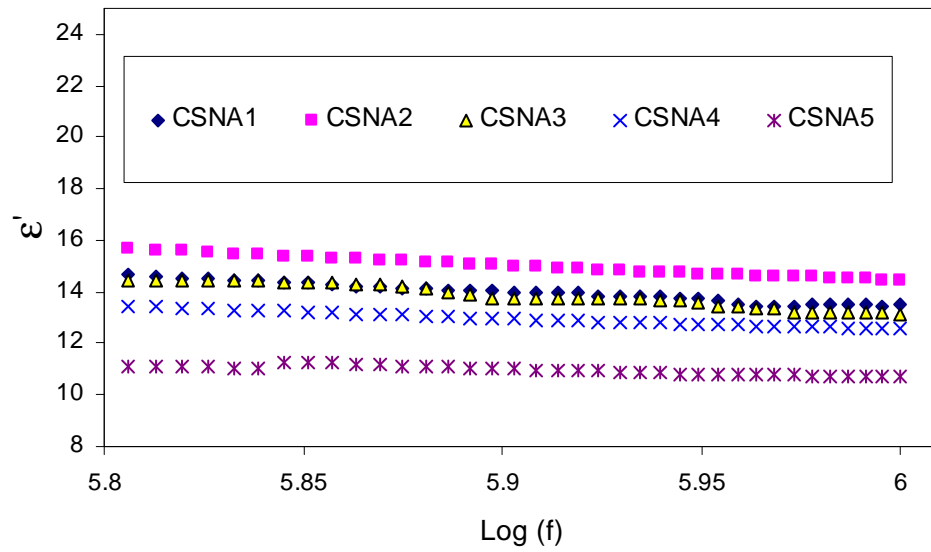
Figure 6.4 Composition dependence of bulk dielectric constant for (1-x)(0.9CS:0.1AgTf)-xAl₂O₃ (0.02 ≤ x ≤ 0.1) NCPEs.

Figure 6.5 demonstrates further relationship between bulk dielectric constant and DC conductivity. It can be seen that the behavior of bulk dielectric constant and bulk DC conductivity almost similar with Al_2O_3 nanoparticle concentration. This result reveal that DC conductivity also is strongly depends on dielectric constant in NCPEs.
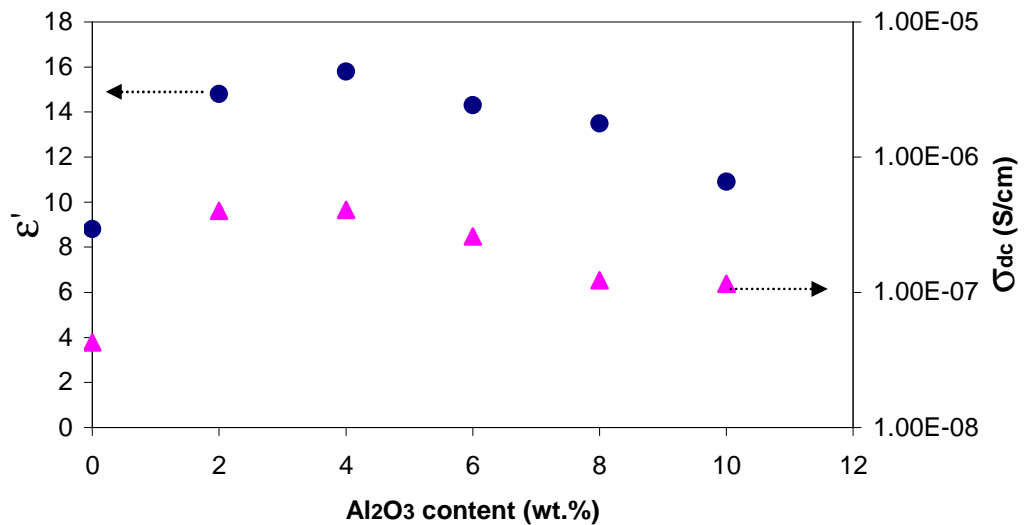
Figure 6.5 Dependence of Bulk dielectric constant and DC conductivity of chitosan:AgTf (CSA6) on Al₂O₃ concentration.

The frequency dependence of dielectric constant for CSNA2 (highest conducting sample) at different temperatures is presented in Fig. 6.6. From the figure, it can be seen that the dielectric constant decreases with increasing frequency. The high value of ε', at low frequencies is due to the electrode polarization. However, the high frequency region of dielectric constant which represents the bulk (intrinsic material property) properties is almost frequency independent but temperature dependent as depicted in Fig. 6.7. It is interesting to note that with increasing temperature the dielectric dispersion shifts to high frequency part. This can be ascribed to high charge carrier build up at high temperature at the electrode/electrolyte interface and thus the dominance of EP effect. Compared to the CSA6 solid polymer electrolyte, the CSNA2 bulk dielectric constant is higher at all temperatures for example at 333 K the bulk dielectric constant of CSNA2 (24) is about two times greater than the bulk dielectric constant of CSA6 (12.9) .
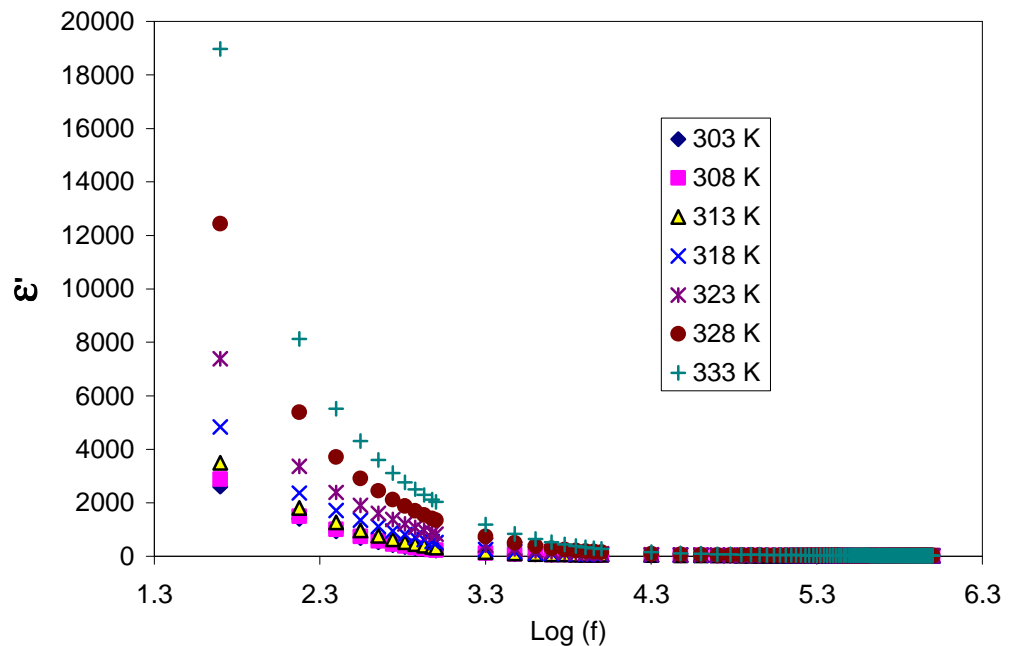
Figure 6.6 Frequency dependence of dielectric constant at different temperatures for CSNA2 sample.
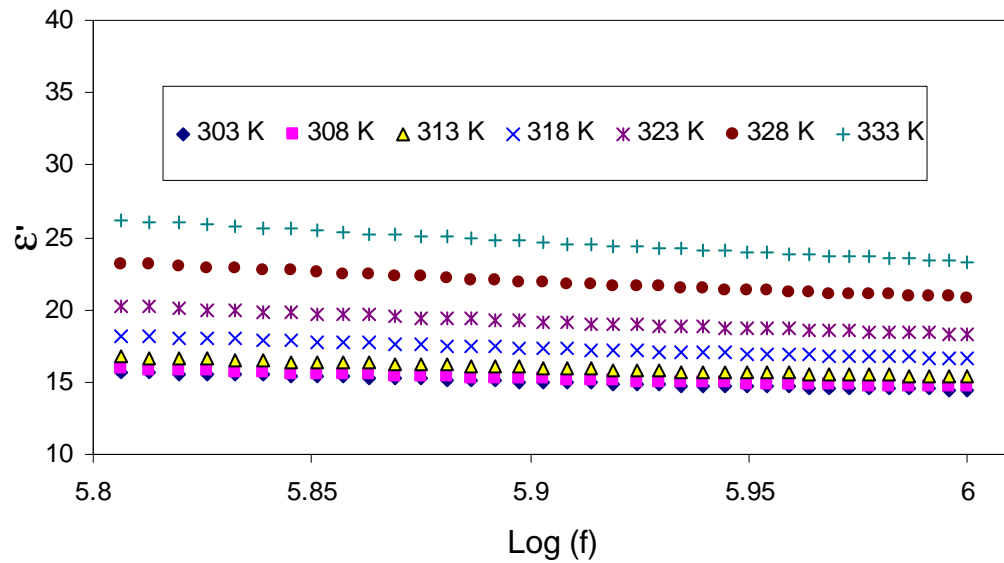
Figure 6.7 Frequency dependence of bulk dielectric constant at different temperatures for CSNA2 sample.

From the above results it can be understood that the bulk DC conductivity and bulk dielectric constant are strongly correlated as we have seen for solid polymer electrolytes. Thus we can satisfy the Petrowsky and Frech hypothesis (2009, 2010) on nano-composites also. The smooth curve between DC conductivity and dielectric constant at different temperatures can be seen for CSNA2 as shown in Fig 6.8.

This smooth curve in the temperature range can be viewed as an empirical description of the dependence of DC conductivity on the dielectric constant (ε') at different temperatures. An increase in dielectric constant means an increase in charge carrier concentration and thus an increase in DC conductivity ($\sigma = \Sigma qn\mu$). The concentration dependence of bulk dielectric constant and DC conductivity (Fig.6.5) and the smooth curve (Fig.6.8) completely reveal that DC conductivity dependence on both temperature and dielectric constant. One point of conductivity can be selected on this curve as a reference to scale the DC conductivity.
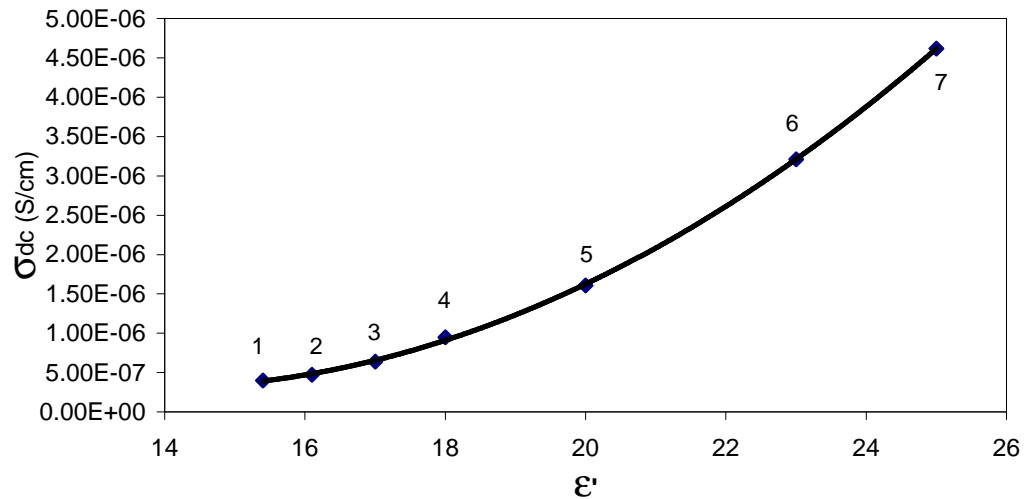
Figure 6.8 DC conductivity dependence on dielectric constant at, (1) 303, (2) 308, (3) 313, (4) 318, (5) 323, (6) 328 and (7) 333 K for CSNA2 sample.

Figure 6.9 depicts the compensated Arrhenius behavior for the temperature dependence of conductivity for the scaled CSNA2 nano-composite polymer electrolyte. It can be seen that the temperature dependence is linear with a regression value of 0.97. The slope gives an activation energy of 0.978 which is almost the same compared to the calculated one from normal Arrhenius relation. This activation energy was used to calculate the pre-exponential factor.
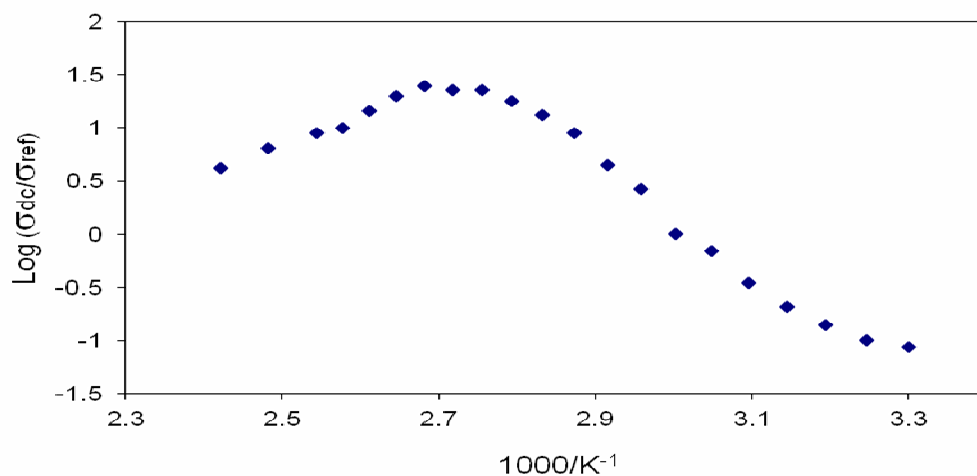
Figure 6.9 Compensated Arrhenius equation plotted against the reciprocal temperature for CSNA2 system.

Figure 6.10 shows the temperature and dielectric constant dependent of pre-exponential factor for CSNA2. It is clear that the pre-exponential factor dose not exhibit a smooth curve with dielectric constant as observed for DC conductivity with dielectric constant. Thus, the NCPEs do not follows the Petrowsky and Frech hypothesis. The pattern for compensated Arrhenius and normal Arrhenius plot, are similar and again reveals that nano-composite electrolytes based on chitosan do not follows the Petrowsky and Frech hypothesis.
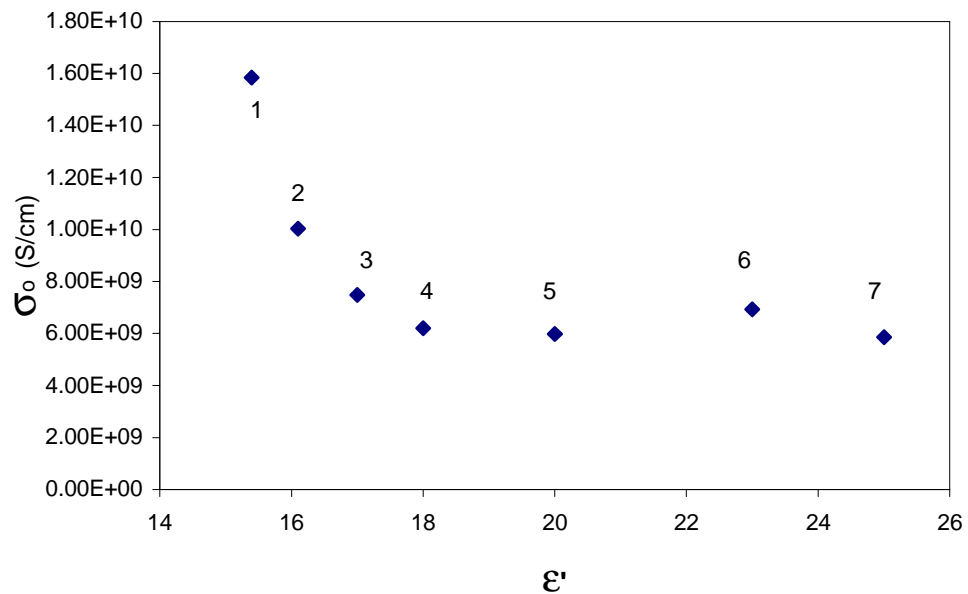
Figure 6.10 Temperature and dielectric constant dependent of pre-exponential factor (σ_o) at (1)303, (2) 308, (3) 313, (4) 318, (5) 323, (6) 328 and (7) 333 K for CSNA2 system.

Figure 6.11 depicts the variation of dielectric loss with frequency at selected temperatures for CSNA2 system. Compared to dielectric constant the dielectric loss value is so large. The dielectric loss becomes very large at lower frequencies due to free charge motion within the material [Malathi et al., 2010].
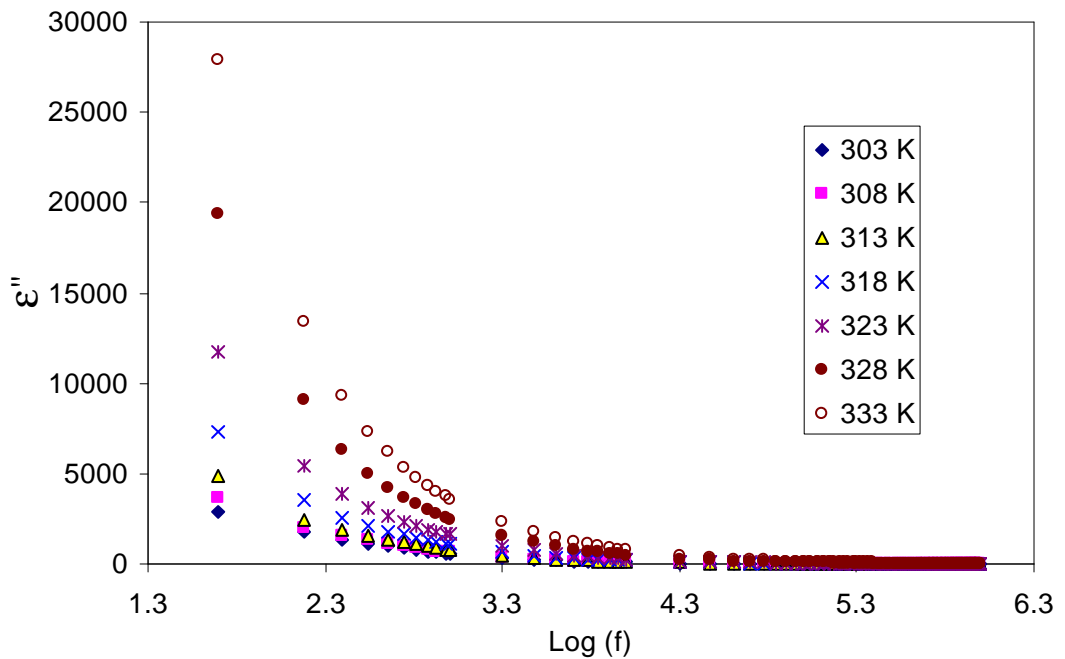
Figure 6.11 frequency dependence of dielectric loss at different temperatures for CSNA2 system.

6.2.2 Frequency dependence of tan δ for NCPE (CSNA2) system

Figure 6.12 shows the variation of loss tangent with frequency at different temperatures for the CSNA2 sample. The tan δ spectrum is characterized by a peak appearing at a characteristic frequency. It can be seen that the tan δ peaks shift towards the higher frequency side with increasing temperature indicating the decrease of the sample's resistance. The shifting of the peaks to higher frequency results in reduced relaxation time. The broad nature of the peaks can be attributed to non Debye type relaxation. In other words, these broad peaks ascribed to the distribution of relaxation times.
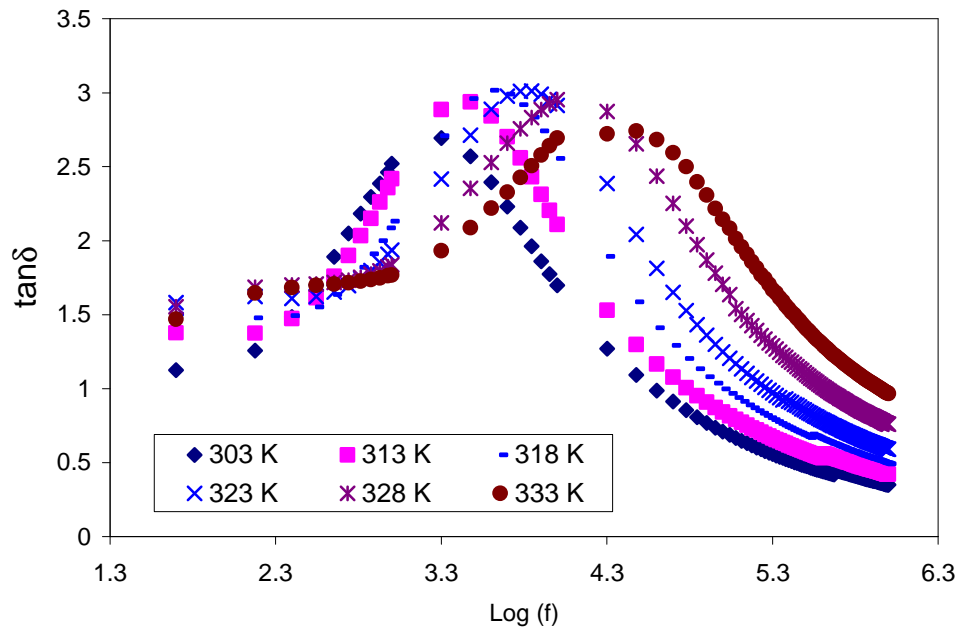
Figure 6.12 Frequency dependence of loss tangent (tanδ) at different temperatures for CSNA2 sample.
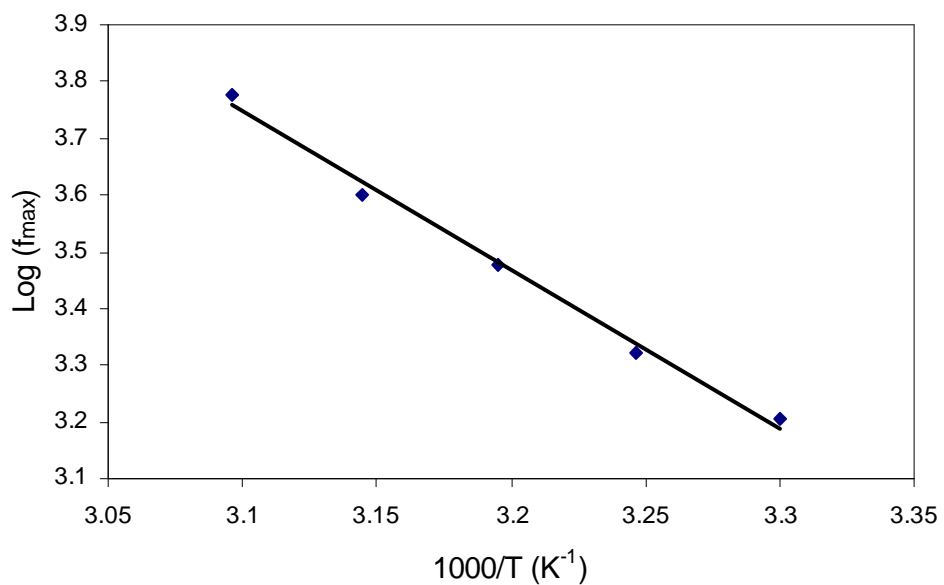
Figure 6.13 Temperature dependence of relaxation frequency for CSNA2 system.

The frequency associated with each peak is known as relaxation frequency. The Log f_{max} –temperature relationship (Fig 6.13) satisfy the Arrhenius equation with the activation energy, $E_a = 0.93$ eV.

6.2.3 Electric modulus analysis of CSNA2: Relaxation processes

Electrical relaxation in ionic conductors can be studied in terms of dielectric modulus to suppress the electrode polarization effect. The low frequency tail of the M′ spectra (Fig. 6.14) can be attributable to a high dielectric constant at low frequencies (EP effect). This can be understood from the relationship between dielectric constant (ε′) and real part of electric modulus ($M' = \varepsilon'/(\varepsilon'^2 + \varepsilon''^2)$). The increase of M′ spectra at higher frequencies predicts the relaxation processes which may appear as a peak in the imaginary part.
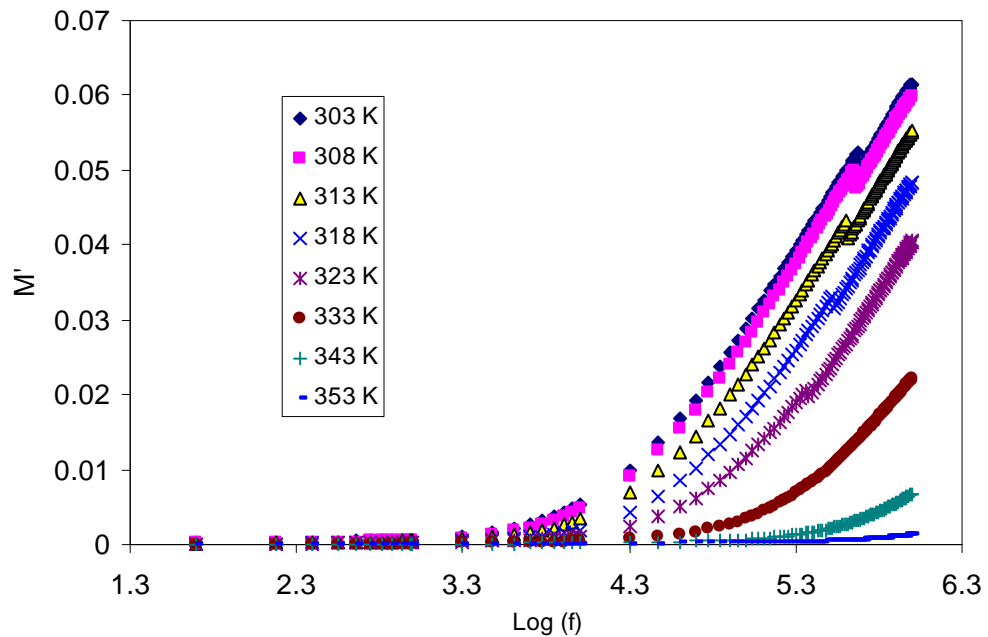
Figure 6.14 Frequency dependence of M' at different temperature for CSNA2 sample.

Figure 6.15 depicts the imaginary part of electric modulus as a function of frequency at selected temperatures for CSNA2 sample. It is obvious that the maximum peaks shifts to high frequencies with increasing temperature. These peaks indicate the fact that our samples are ionic conductors.
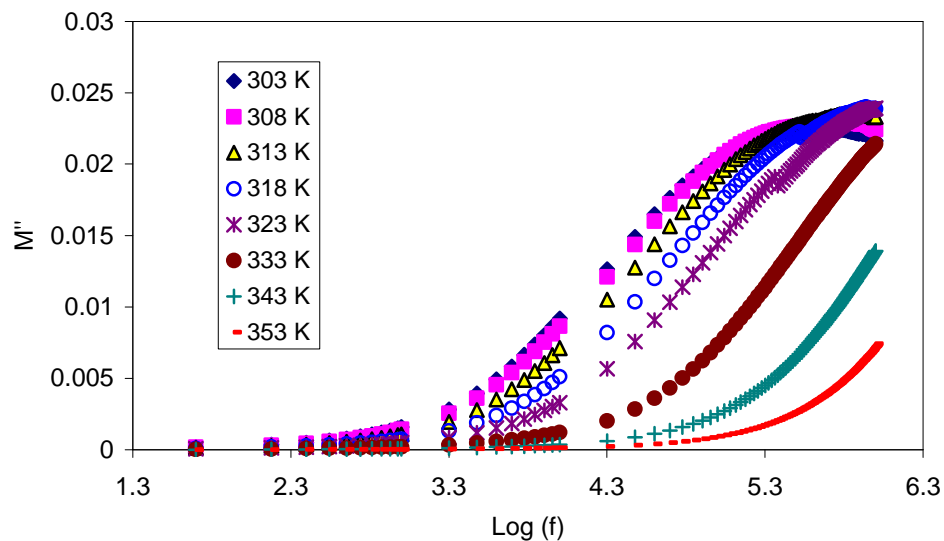
Figure 6.15 Frequency dependence of M'' at different temperature for CSNA2 sample.

In dielectric measurements, the material is exposed to an alternating electric field, which is generated by applying a sinusoidal voltage; this process causes alignment of dipoles in the material, which results in polarization. In polymeric materials the dipoles on the side chain of the polymer backbone can produce dipolar polarization and as well as the existence of ion translational diffusion [Mohomed et al., 2006]. The appearance of peak maximum in the imaginary part of electric modulus reveals the sample is ion conductor. Argant plots (M'' vs M') can be used to investigate the relaxation dynamics of the translational diffusion of ions. Ayesh (2010) has shown that if the Argand plot between imaginary part (M'') versus real part (M') of electric modulus has semicircular behavior

then the relaxation is due to conductivity relaxation process, otherwise, it is due to viscoelastic relaxation (or polymer molecular relaxation) [Ayesh, 2010]. The conductivity relaxation possesses properties very different from the viscoelastic relaxations present in polymers. The conductivity relaxation corresponds to the model of a Debye process having a single relaxation time, whereas viscoelastic relaxations are known to exhibit a distribution of relaxation times [Mohomed et al., 2005]. Figure 6.16 shows the Argand plot for CSNA2 sample at different temperatures. All plots shows incomplete semicircular arc as a result of distribution of relaxation times, i. e., non-Debye behavior and consequently the relaxation processes are due to viscoelastic relaxation.
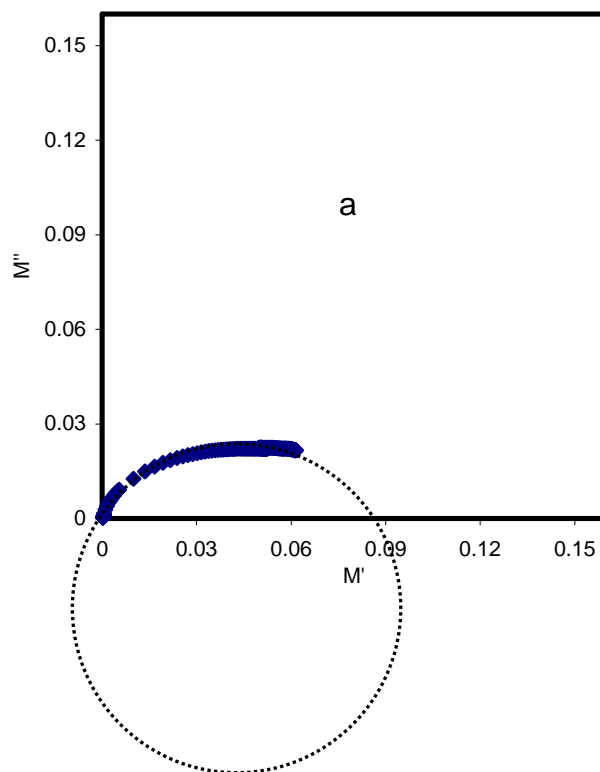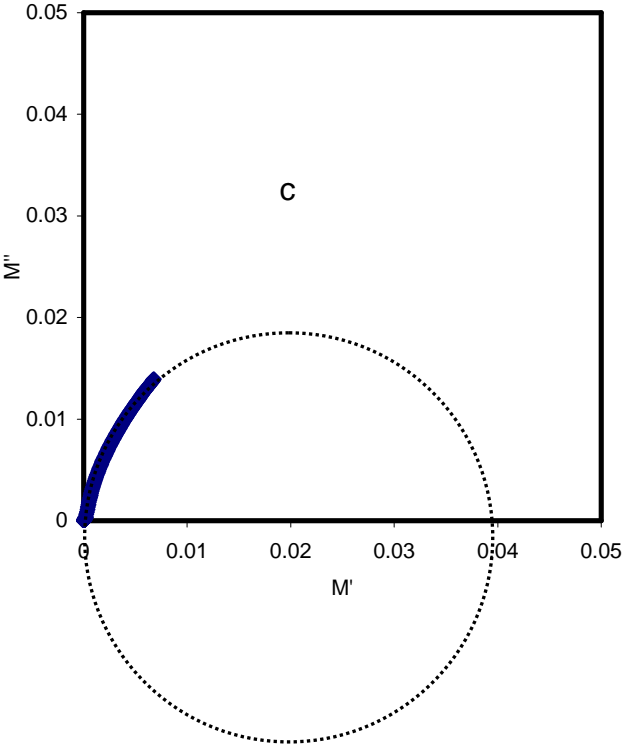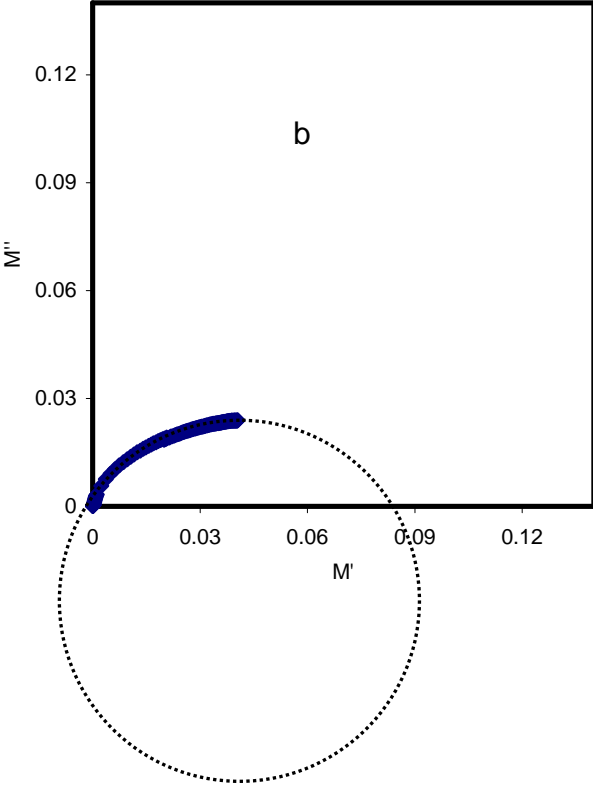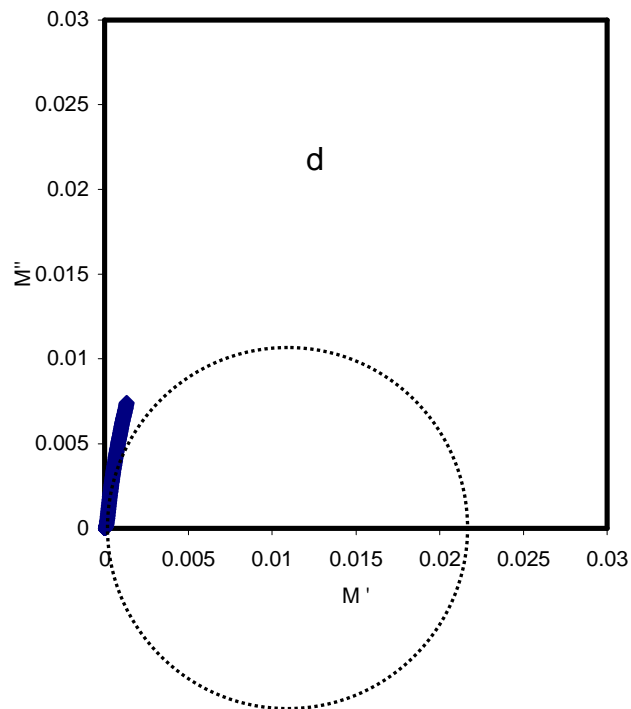
Figure 6.16 Argand plots for NCPE (CSNA2) at (a) 303 K, (b) 323 K, (c) 343 K and (d) 353 K.

6.2.4 Correlation between impedance and AC conductivity (σ_{ac}) in NCPEs (CSNA2).

Fig. 6.17(a-f) represents the complex impedance plots of the CSNA2 sample at different temperatures. The plots show two semicircles at high and intermediate frequencies and a tilted spike at low frequency due to electrode polarization effect. It is clear that with increasing temperature the high semicircle (bulk property) vanishes and the spike region increases strongly. The spike region is due to the large accumulation of charge at the electrode/sample interface. It can be seen that at high temperatures (Fig. 6.17(e-f)) the high frequency semicircle corresponds to bulk ionic conduction is almost disappear.
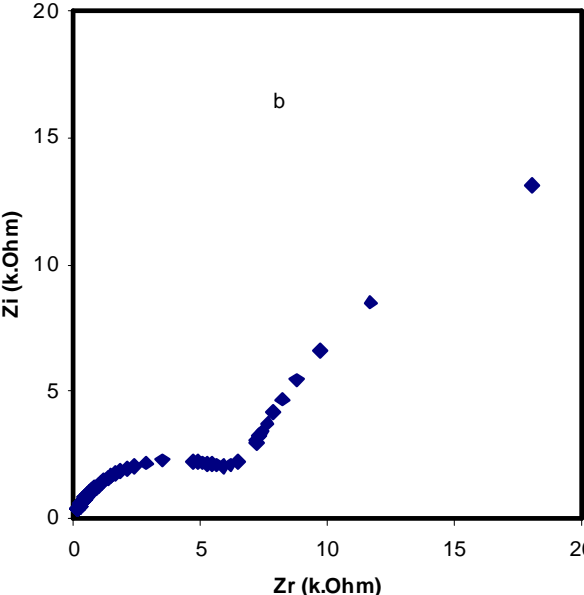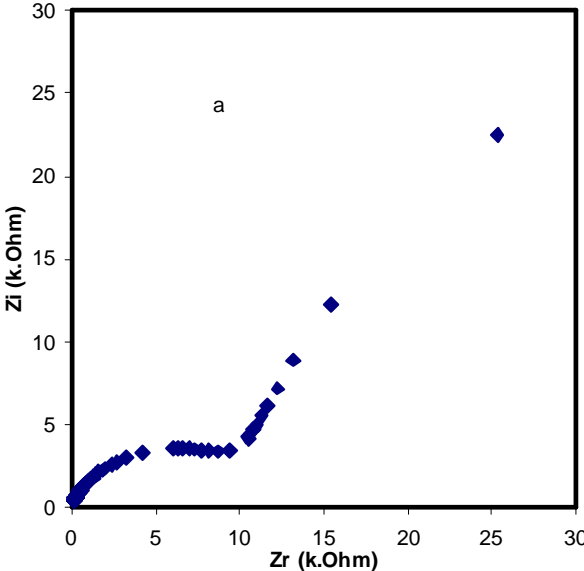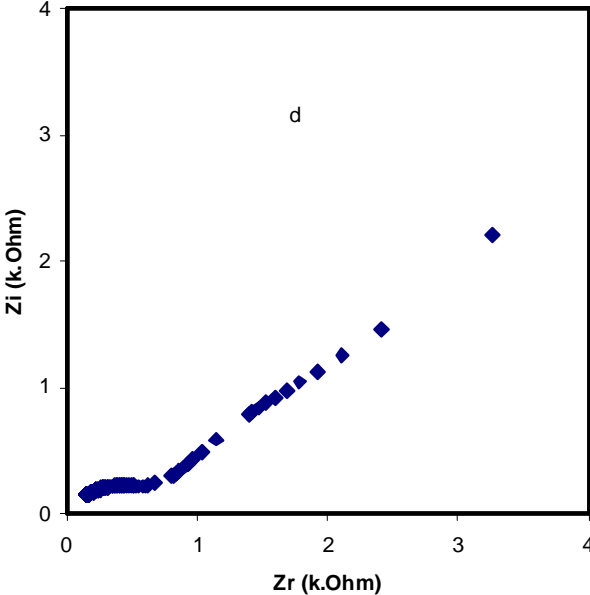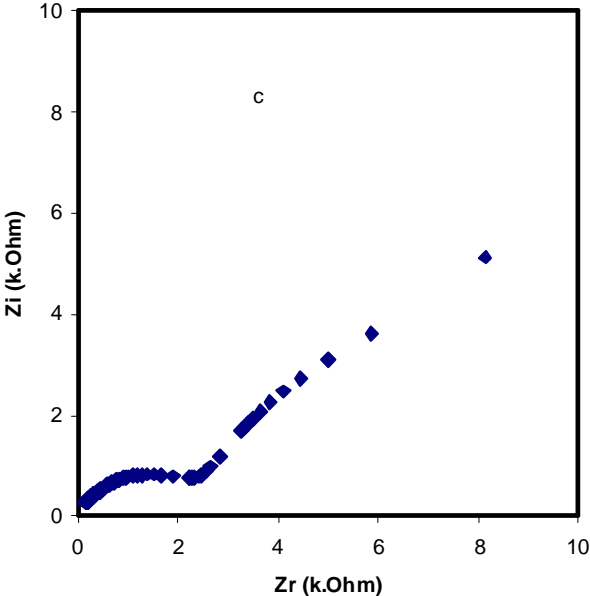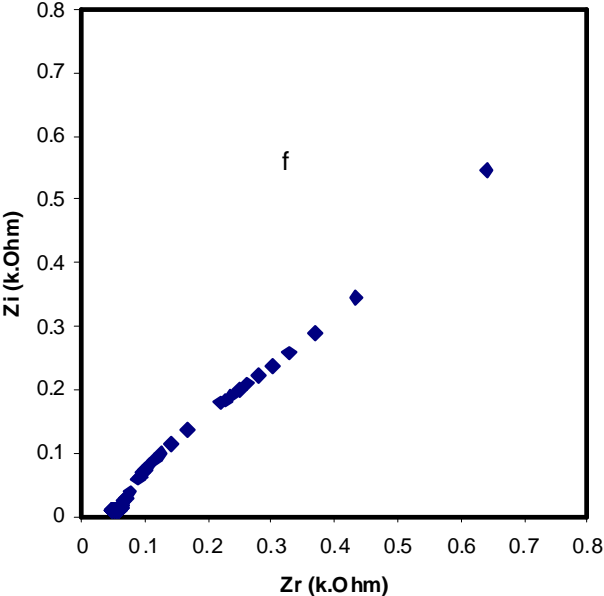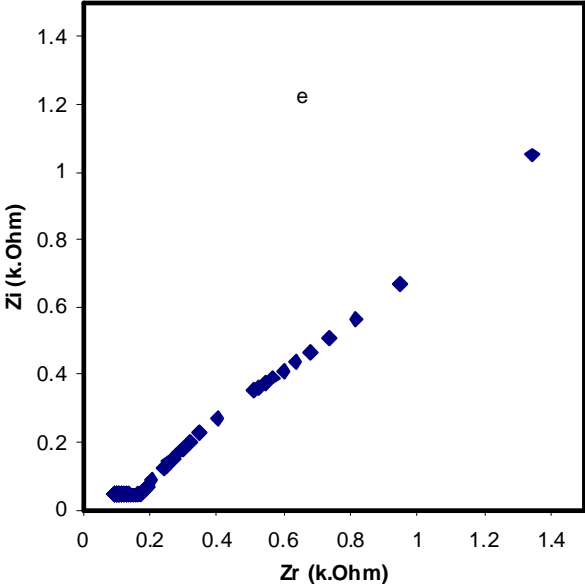
Figure 6.17 Impedance plots for NCPE (CSNA2) at (a) 303 K, (b) 313 K, (c) 323 K, (d) 333 K, (e) 343 K, and (f) 353 K.

A typical conductivity-frequency spectrum shown in Fig. 6.18(a-d) exhibits three distinguish regimes; low frequency dispersion, an intermediate plateau and conductivity dispersion at high frequency from 303 K to 333 K. The variation of conductivity in the low frequency region is attributed to the polarization effects at the electrode/electrolyte interface. In the intermediate frequency region, conductivity is almost found to be frequency independent and equal to dc conductivity and at the high frequency region, the conductivity increases with frequency. The frequency dependence of electrical conductivity at the high frequency region obeys Jonscher's power law. The direct correlation of AC conductivity spectra to Nyquist plots reveal that the AC dispersion strongly relates to the bulk property of the sample. It can be seen from Nyquist plots that at higher temperatures the high frequency semicircle disappears as a result of high accumulation of charges. Also at high temperatures the AC dispersion also decreases.
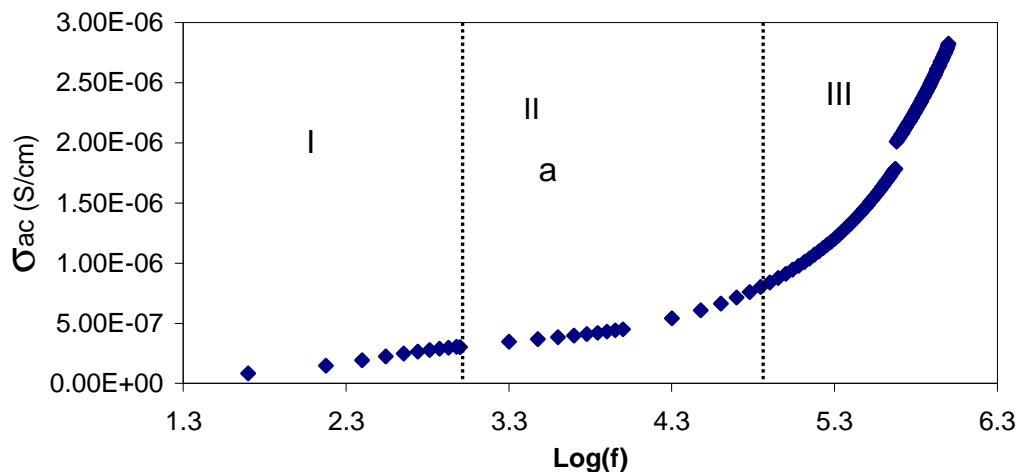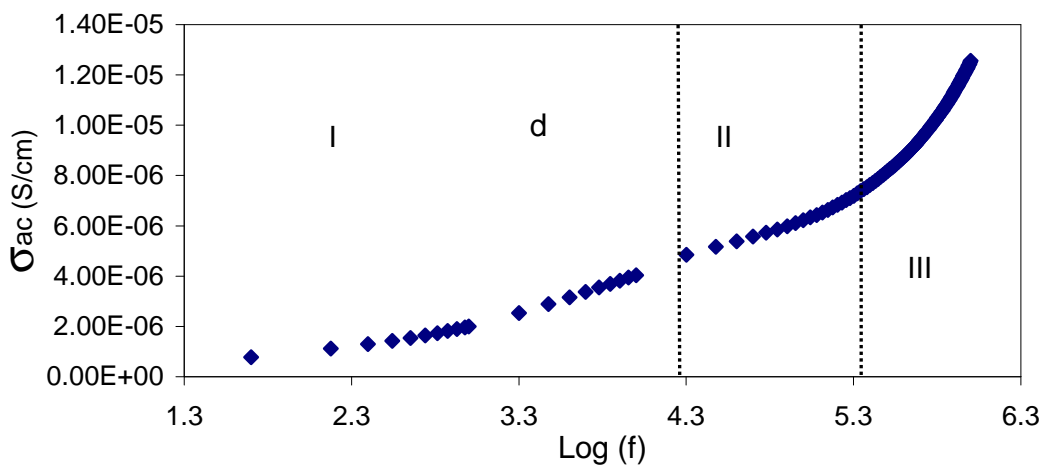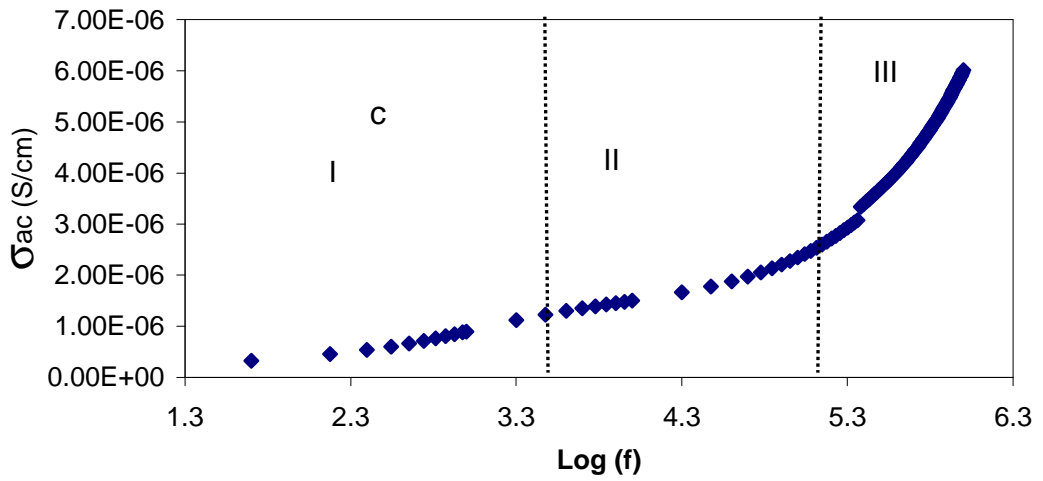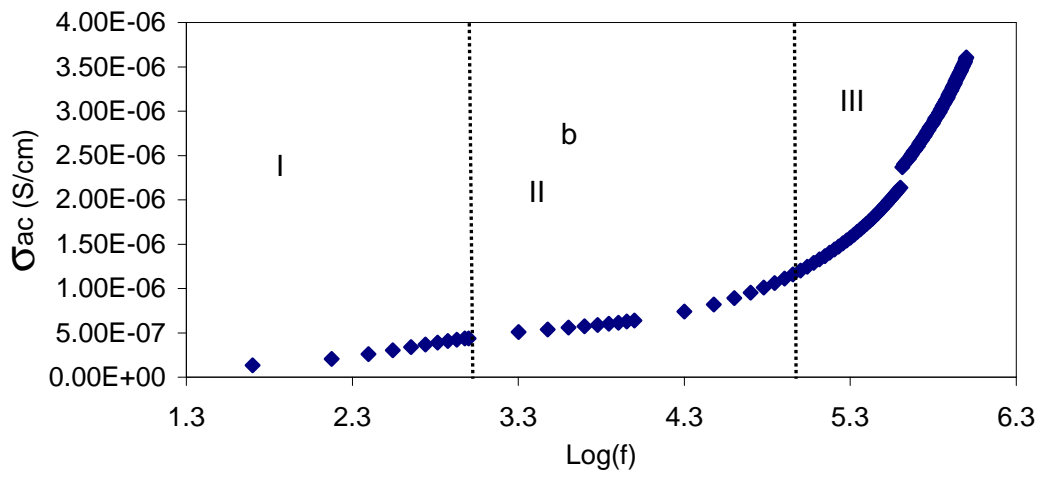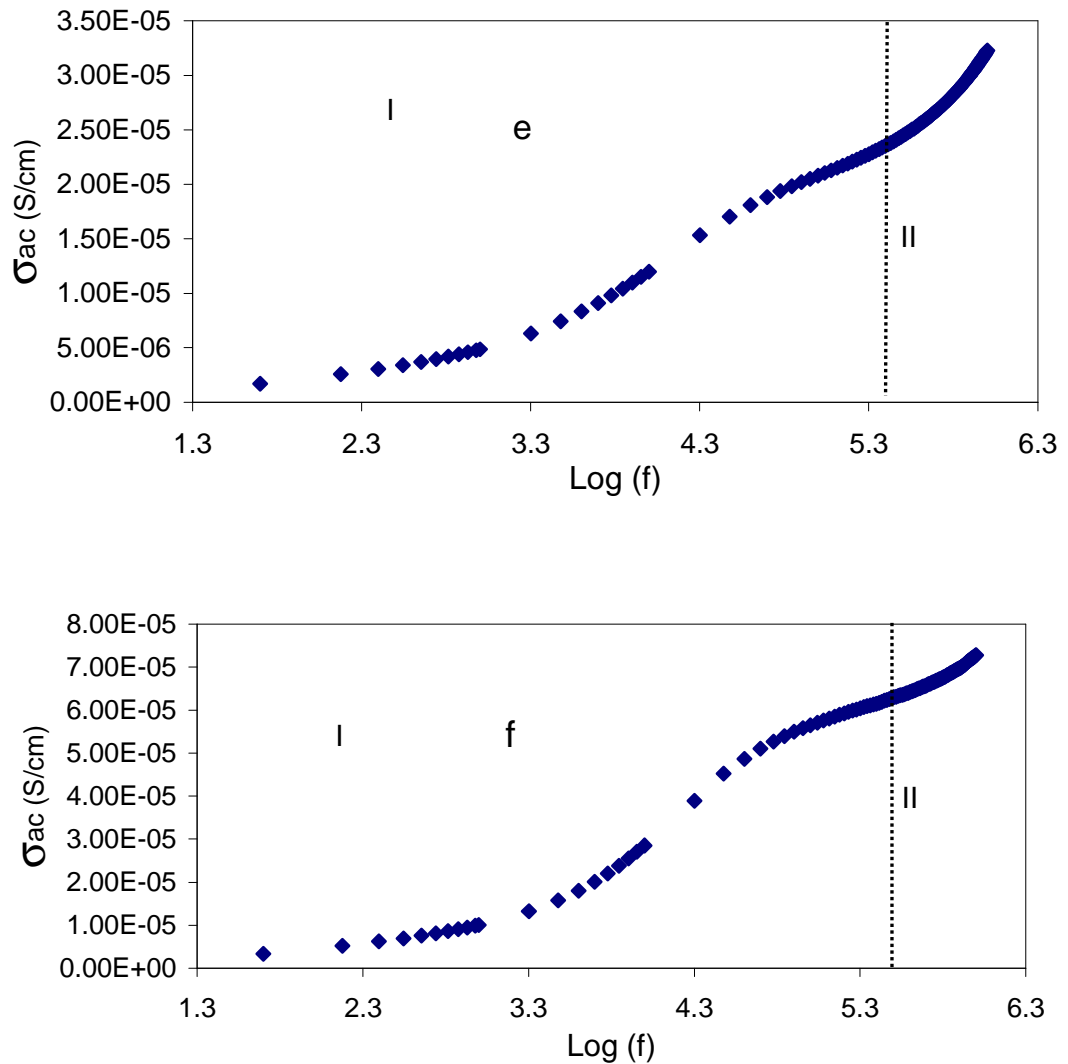
Figure 6.18 AC conductivity spectra for NCPE (CSNA2) at (a) 303 K, (b) 313 K, (c) 323 K, (d) 333 K, (e) 343 K, and (f) 353 K.

Figure 6.19 depicts the variation of frequency exponent (s) with temperature. It can be seen that the s value decrease with increasing temperature to a minimum value and then increases slightly with temperature. According to QLPT model [Faraga et al., 2010], the exponent s depends on both frequency and temperature and drops with rising temperature to a minimum value and then increases slightly, as temperature rises. Thus the ion conduction in CSNA2 system follows the OLPT model.
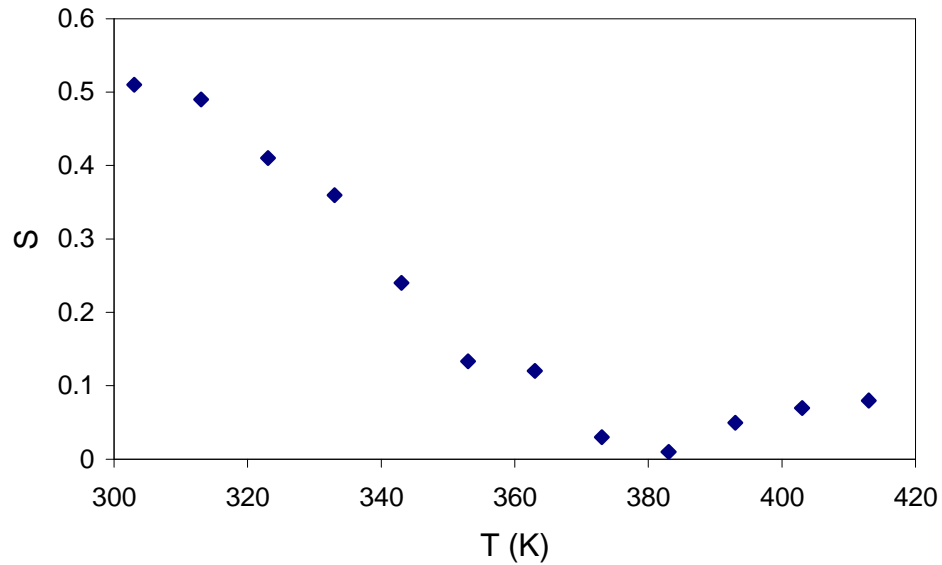
Figure 6.19 Temperature dependence of the frequency exponent s for CSNA2 system.

6.3 Electrical/Dielectric properties of NCPEs based on (1-x)(0.9CS:0.1NaTf)-xAl$_2$O$_3$ (0.02 ≤ x ≤ 0.1)

6.3.1 DC conductivity and Dielectric analysis of NCPEs based on (1-x)(0.9CS:0.1NaTf)-xAl$_2$O$_3$ (0.02 ≤ x ≤ 0.1)

The variation of DC conductivity of CS:NaTf (CSB6) with various concentration of Al$_2$O$_3$ nanoparticles is depicted in Fig 6.20. It can be seen that the DC conductivity increased by addition 2 to 4 wt.% of Al$_2$O$_3$ nanoparticle and thereafter decreased at 6 wt.% and then increased again for high filler concentration (8 to 10 wt.%). According to Dissanayake et al., (2003), the decrease of DC conductivity can be due to the blocking effect and the increase of conductivity at higher filler content can be due to the fact that the filler grains get close enough to each other at higher concentrations so that the high conducting regions in the vicinity of the grain surfaces start to get interconnected. The migrating ionic species can now travel along and between these interconnected high conducting pathways giving rise to the second increase in the conductivity (8 to 10

wt.%). Compare to CS:NaTf (CSB6) system the DC conductivity of (1-x)(0.9CS:0.1NaTf)-xAl$_2$O$_3$ (0.02 ≤ x ≤ 0.1) compositions is two order increased. The increase in DC conductivity can be ascribed to the dielectric constant enhancement as can be seen later.
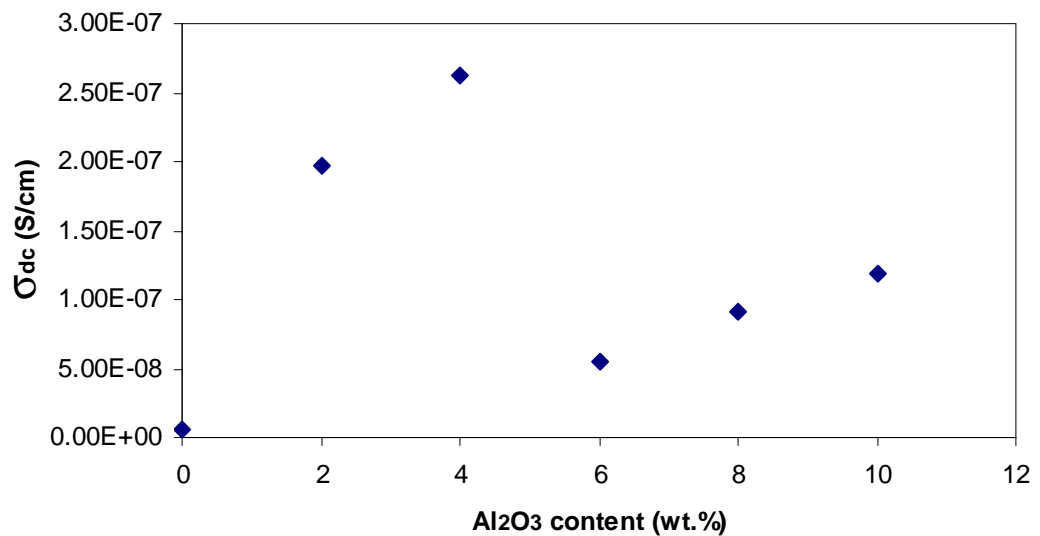
Figure 6.20 The ionic conductivity of chitosan:NaTf (CSB6) with various concentration of Al$_2$O$_3$.

Figure 6.21 shows temperature dependent conductivity of different nanocomposite solid electrolyte samples. It is clear from the plots that the temperature dependence of conductivity follows the Arrhenius behavior for the compositions from 2 to 10 wt.% at low temperaute (303 to 333 K). However they did not follow the Arrhenius behavior for all the compositions at higher temperatures. Similar behavior were reported for PEO:LiTf:Al$_2$O$_3$ composite polymer electrolyte [Dissanayakea et al., 2003]. The bend in the curve has been observed in ionically conducting polymers and has been explained invoking the concept of free volume [Karan et al., 2008]. It is interesting to note that the curve obtained for the highest filler concentrations (10 wt. %) seems to maintain linearity quite well up to the highest temperatures. According to Osińska et al., (2009)

the high filler load helps to prevent ionic transport deterioration at higher temperatures. They explained this phenomenon by assuming that an additional ion transport mechanism occurs when the filler particles become more and more packed in the composite membrane. The decrease of DC conductivity at a particular temperature for all the compositions again can be ascribed to the phase transition of alumina nanoparticles. The calculated activation energy at low temperature (linear part) for the highest conducting sample (CSNB2) is equal to 1.01 eV.
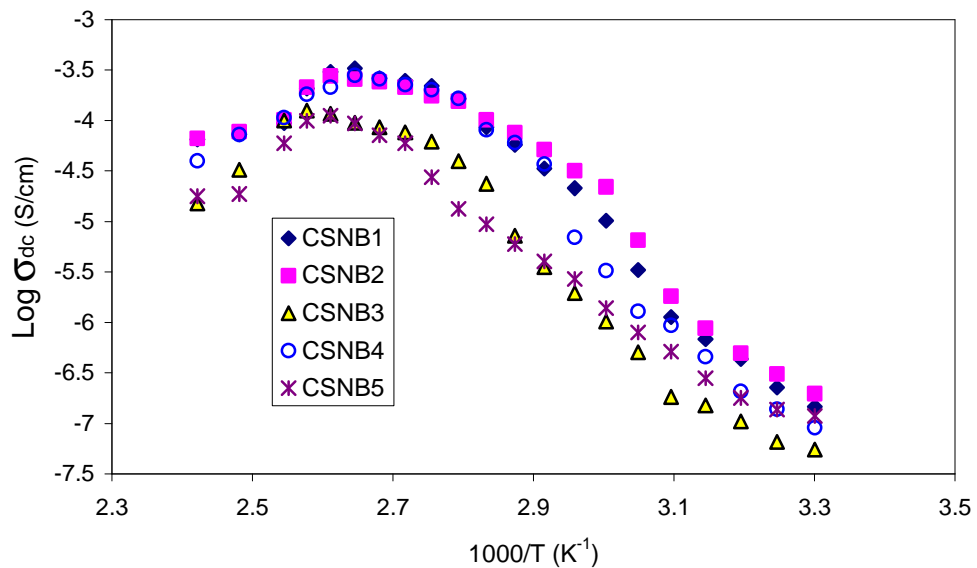
Figure 6.21 temperature dependence of ionic conductivity of (1-x)(0.9CS:0.1NaTf)-xAl$_2$O$_3$ (0.02 ≤ x ≤ 0.1) NCPEs.

Dielectric constant is directly related to the capacitance (C) of the sample ($\varepsilon' = C/C_o$). The high dielectric constant of the sample means a high charge carrier density. Figure 6.22 shows the frequency dependent of dielectric constant for different alumina concentrations. It can be seen that dielectric constant increases with decreasing frequency. This is because at low frequency the dipoles and charge carriers have

sufficient time to orient in the direction of the applied electric field. Consequently large amounts of charge carriers build up at the electrode/electrolyte interface and produces electrode polarization, which suppresses the high frequency dielectric properties (bulk property).
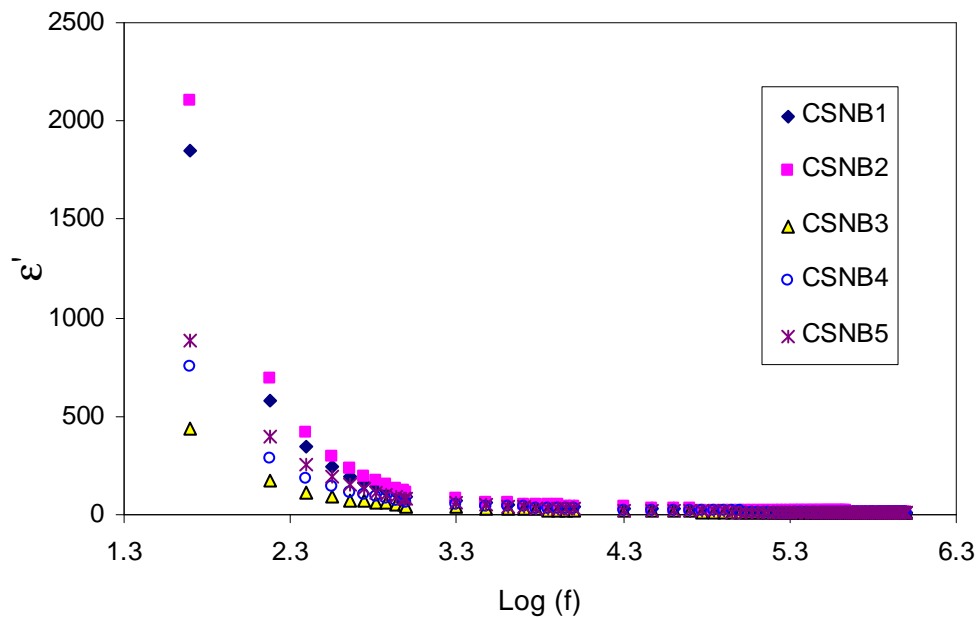
Figure 6.22 Composition dependence of dielectric constant for $(1-x)(0.9CS:0.1NaTf)-xAl_2O_3$ ($0.02 \leq x \leq 0.1$) NCPEs.

Figure 6.23 shows the separated bulk dielectric constant for various concentrations of alumina nanoparticles. It is obvious that the bulk dielectric constant like bulk DC conductivity is strongly affected by the alumina concentration. These results reveal the role of dielectric constant enhancement on DC conductivity in nano-composite polymer electrolytes. The complete relationship between bulk DC conductivity and bulk dielectric constant can be achieved from Fig. 6.24. It can be seen that the behavior of Bulk dielectric constant and bulk DC conductivity almost the same with Al_2O_3 concentration.
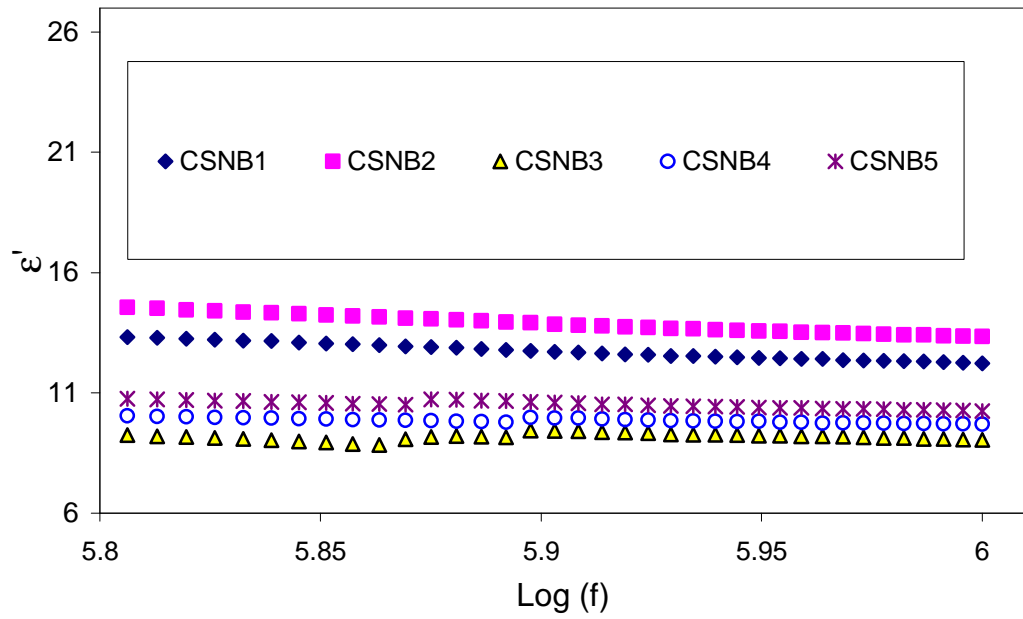
Figure 6.23 Composition dependence of bulk dielectric constant for (1-x)(0.9CS:0.1NaTf)-xAl$_2$O$_3$ (0.02 ≤ x ≤ 0.1) NCPEs.
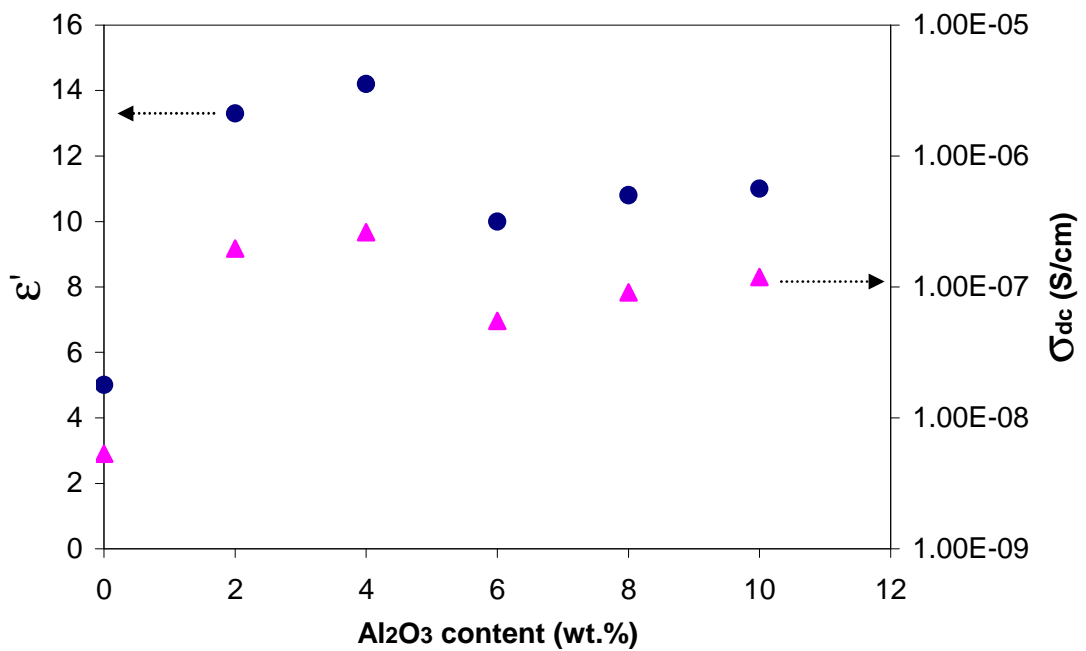
Figure 6.24 Dependence of bulk dielectric constant and DC conductivity of chitosan:NaTf (CSB6) on Al$_2$O$_3$ concentration.

The dielectric constant study at different temperatures may give further information on the relationship between bulk DC conductivity and dielectric constant. Figure 6.25 shows the dielectric constant as a function of frequency at different temperatures. It can be seen that with increasing temperature the dielectric constant also increased. The large value of dielectric constant (ε') at low frequency is attributable to electrode polarization (EP) effect which suppressed the high frequency dielectric constant to a single curve.
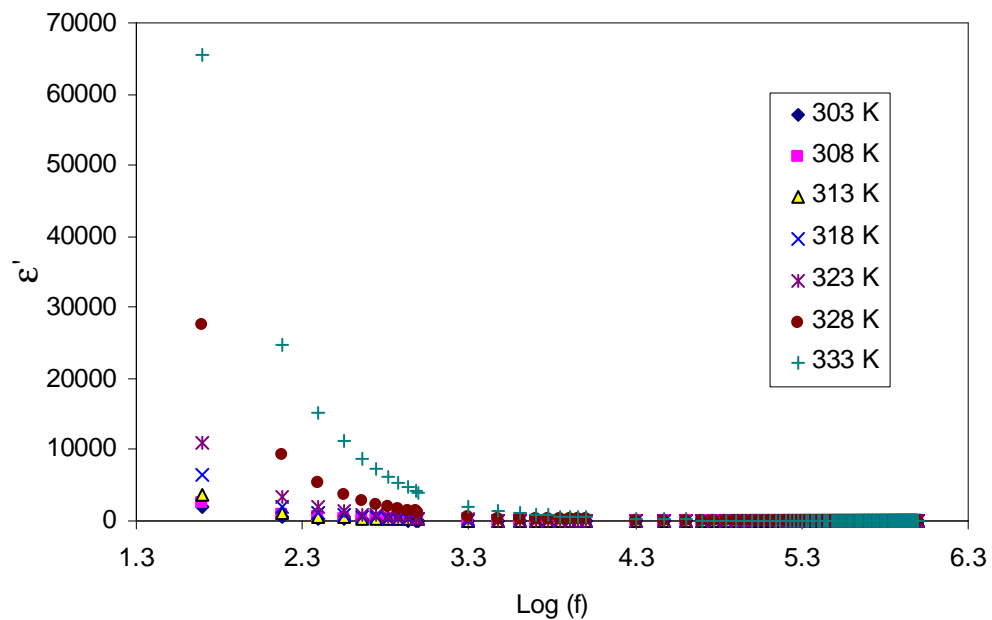
Figure 6.25 Frequency dependence of dielectric constant at different temperatures for CSNB2 system.

Figure 6.26 shows the frequency dependence of the bulk dielectric constant at selected temperatures. It is interesting to note that the bulk dielectric constant is also temperature dependent like low frequency dielectric constant. We know that the bulk DC conductivity and bulk dielectric constant are extracted from the high frequency semicircle. Thus the DC conductivity must also be strongly dielectric constant

dependent. The slight inclination of the bulk dielectric constant can be ascribed to the

EP dominance at high temperature which can be seen Cole- Cole (Z_i-Z_r) study.
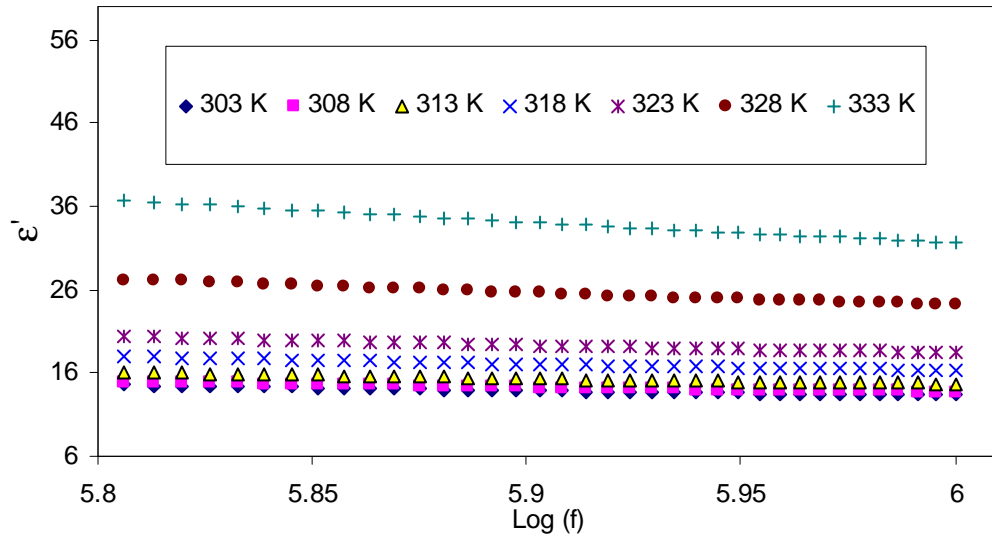
Figure 6.26 Frequency dependence of bulk dielectric constant at different temperatures for CSNB2 system.

Figure 6.27 shows the DC conductivity as a function of bulk dielectric constant at

different temperatures. It is obvious from the plot that the bulk DC conductivity is

smoothly increased with increasing bulk dielectric constant and the increase in dielectric

constant means an increase in charge carrier concentration at different temperatures.

Thus the dependence of bulk DC conductivity and dielectric constant (Fig. 6.24) on

Al2O3 concentration together with the smooth curve between DC conductivity and

dielectric constant (Fig. 6.27) reveal that DC conductivity is strongly dielectric constant

dependent in NCPEs.

 One point of conductivity can be selected on this curve as a reference to scale the DC

conductivity and study the compensated Arrhenius equation.
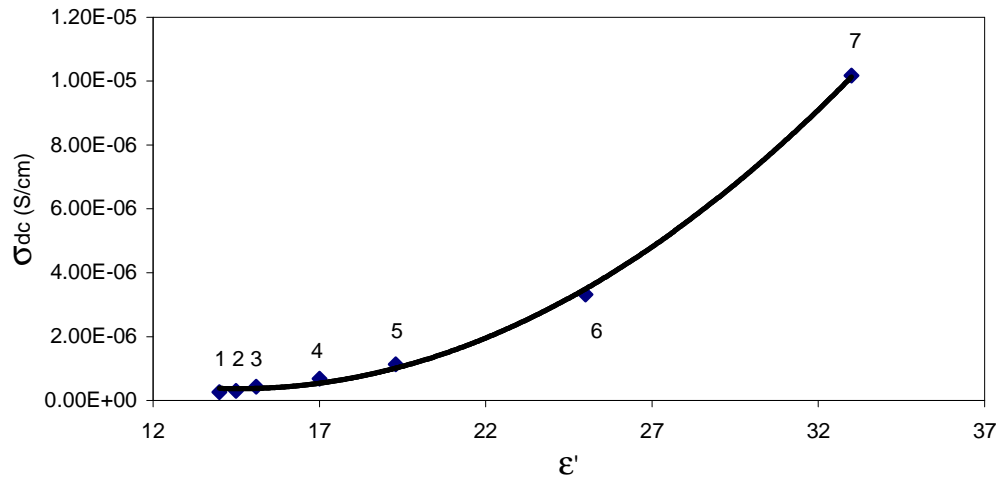
Figure 6.27 DC conductivity dependence on dielectric constant at, (1) 303, (2) 308, (3) 313, (4) 318, (5) 323, (6) 328 and (7) 333 K for CSNB2 system.

Figure 6.28 shows the compensated Arrhenius behavior for CSNB2 sample which exhibits similar behavior with temperature as occurred for DC conductivity (Fig. 6.21). The slope gives activation energy of 1.04 eV in the low temperature region which is almost the same compared to the calculated one from normal Arrhenius relation. This activation energy was used to calculate the pre-exponential factor by dividing the conductivity with the quantity $\exp(-E_a / K_b T)$.
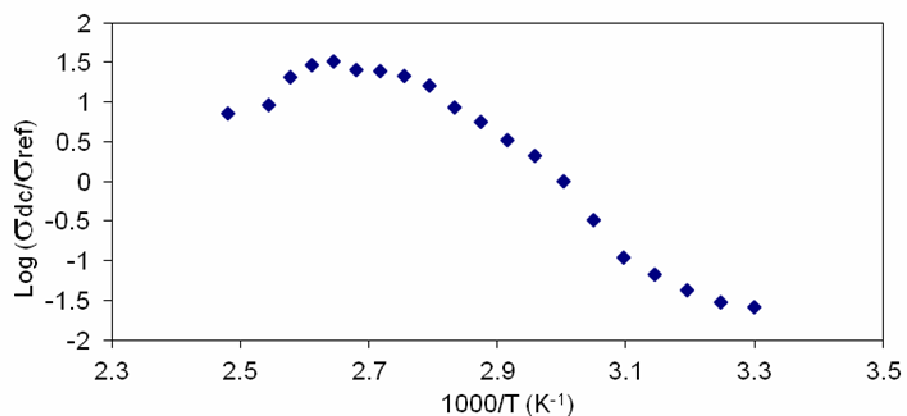
Figure 6.28 Compensated Arrhenius equation plotted against the reciprocal temperature for CSNB2 system.

The temperature and dielectric constant dependence of pre-exponential factor for CSNB2 is shown in Figure 6.29. The absence of smooth curve between the pre-exponential factor and dielectric constant indicated that chitosan based nanocomposite solid electrolyte is also not follows the Petrowsky and Frech hypothesis. Fortunately the second nano-composite solid polymer electrolytes systems $(1-x)(0.9CS:0.1NaTf)-xAl_2O_3$ $(0.02 \leq x \leq 0.1)$ reveal that Arrhenius equation steel applicable. The same pattern of compensated Arrhenius and normal Arrhenius plot again reveals the non-applicability of Petrowsky and Frech hypothesis for nano-composite solid electrolytes based on chitosan.
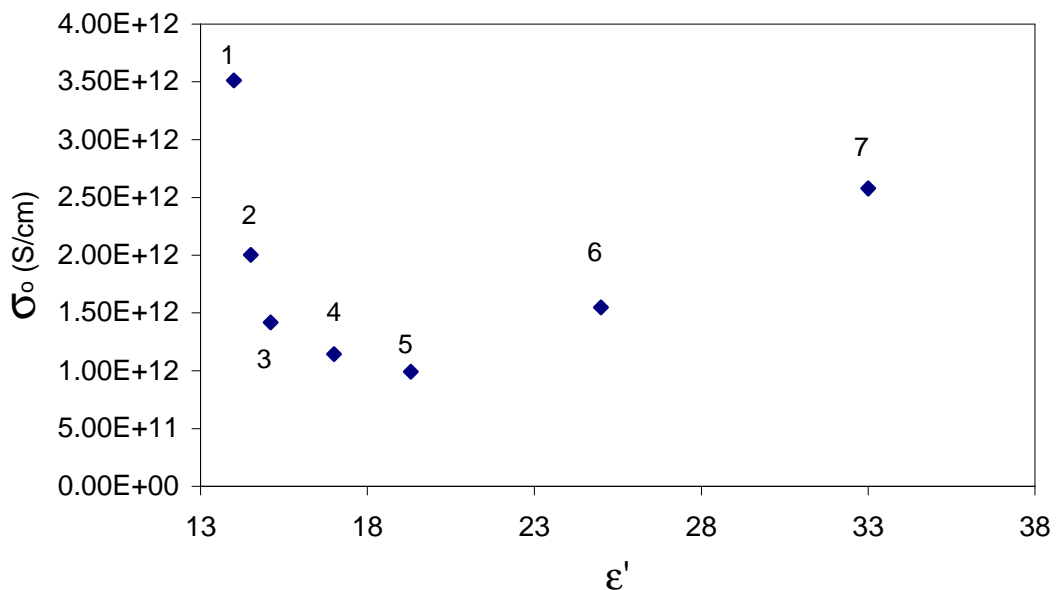
Figure 6.29 Temperature and dielectric constant dependent of pre-exponential factor (σ_o) at (1)303, (2) 308, (3) 313, (4) 318, (5) 323, (6) 328 and (7) 333 K for CSNB2 system.

Figure 6.30 shows the variation of dielectric loss with frequency at selected temperatures for CSNB2 system. The dielectric loss value is very large at low

frequencies due to EP effect. The dispersion of dielectric loss spectra shifts to high frequency part with increasing temperature as a result of high charge carrier dissociation.
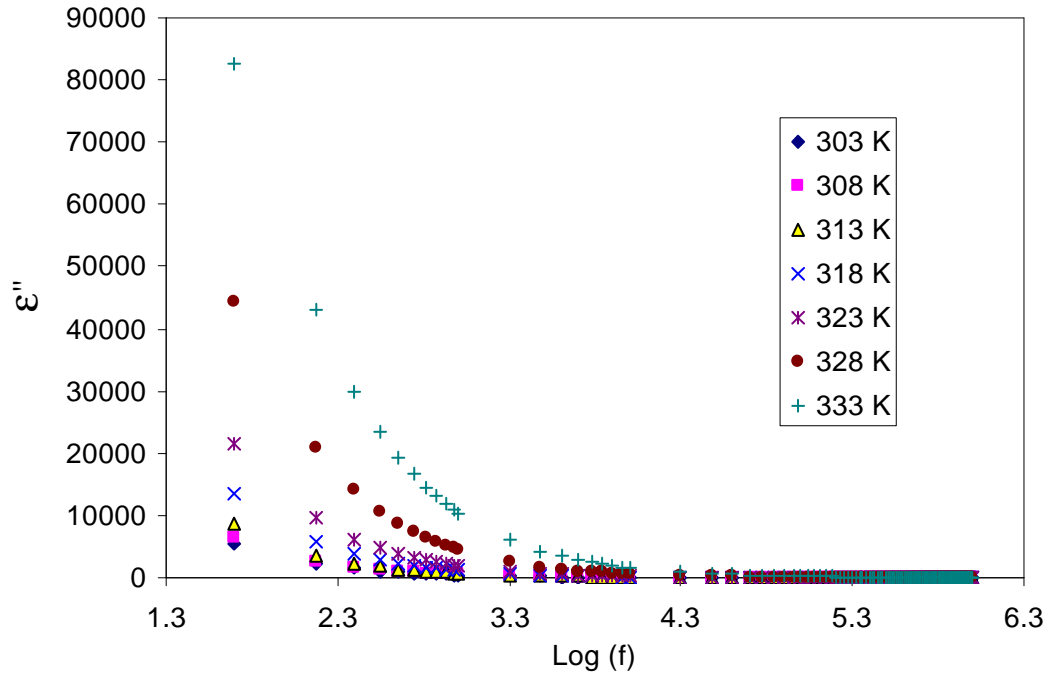
Figure 6.30 frequency dependence of dielectric loss at different temperatures for CSNB2 system.

6.3.2 Frequency dependence of tan δ for NCPE (CSNB2) system

Dielectric loss tangent, tan δ, is an important characteristic, which represents the ratio of dissipation of energy to the stored energy in the material. It is obvious (Fig. 6.31) the tan δ peaks shift to high frequency with increasing temperature. This indicates the decrease of relaxation time and the broadness of the peaks can be ascribed to the distribution of relaxation times.
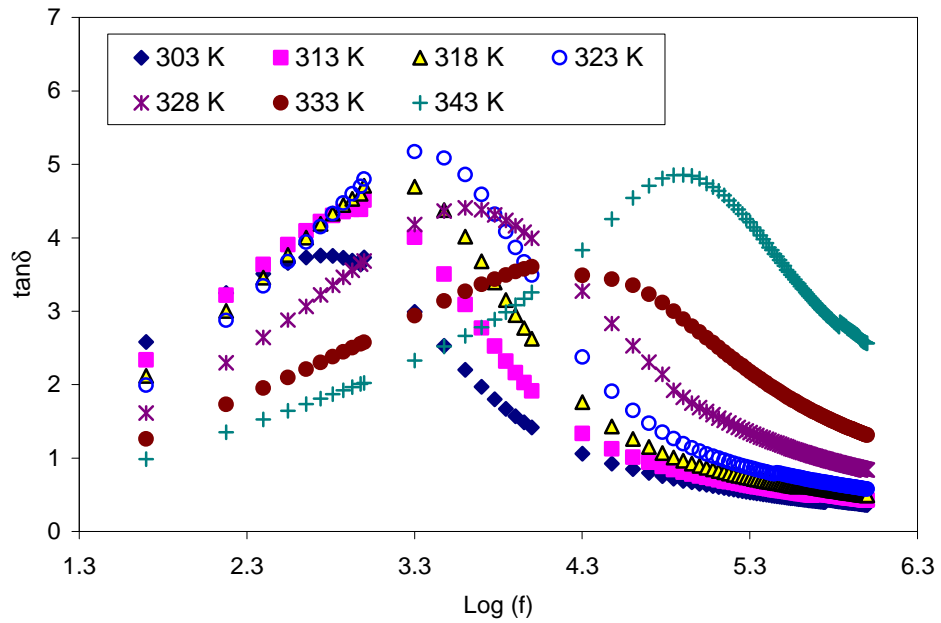
Figure 6.31 Frequency dependence of loss tangent (tanδ) at different temperatures for CSNB2 system.

Figure 6.32 shows the temperature dependence of relaxation frequency. The frequency-temperature relationship gives activation energy 0.987 eV. The regression value is 0.96 indicating that all points lie on almost the same straight line.
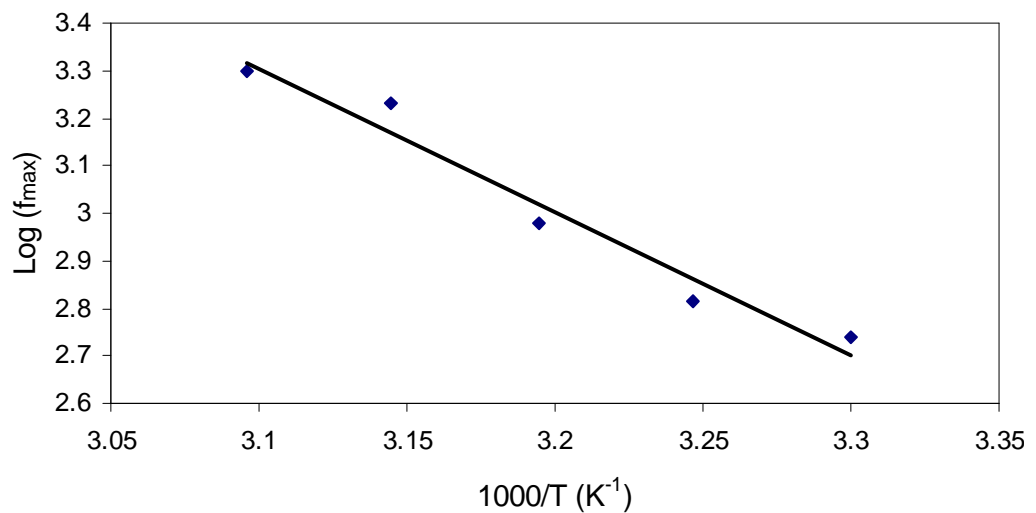
Figure 6.32 Temperature dependence of relaxation frequency for CSNB2 system.

6.3.3 Electric modulus analysis of CSNB2 system: Relaxation processes

The variation of real part (M′) of electric modulus as a function of frequency at selected temperatures is presented Fig 6.33. Due to the EP effect the value of M′ is very small at low frequency. It is clear that the value of M′ increased with increasing frequency.
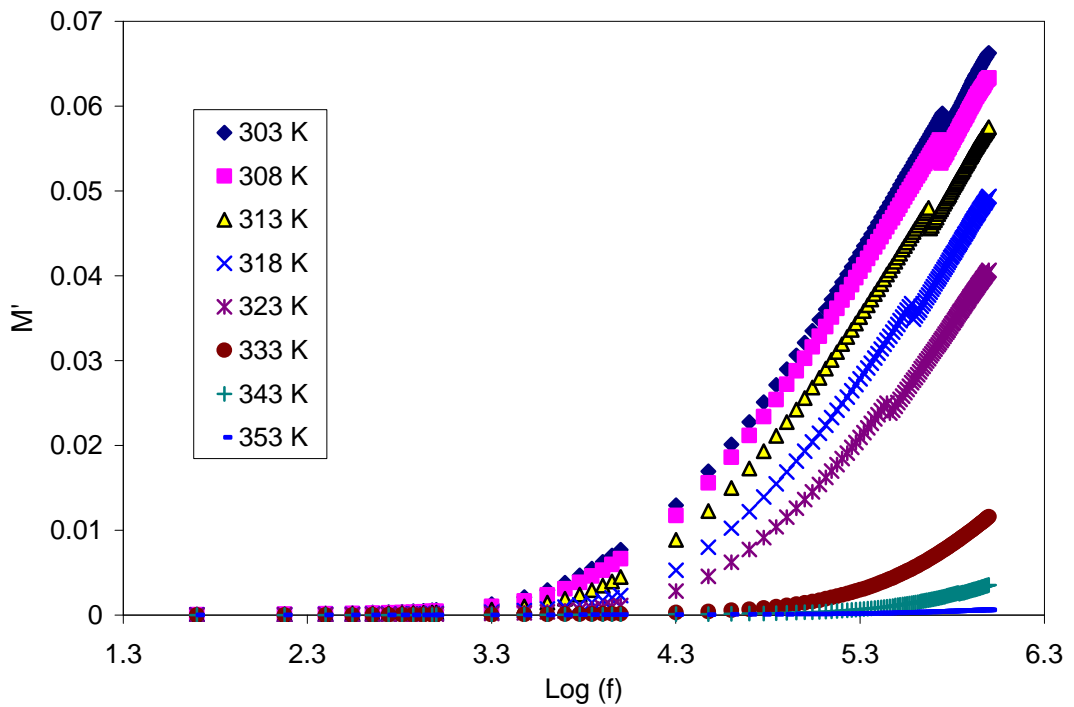
Figure 6.33 Frequency dependence of M' at different temperature for CSNB2 sample.

The variation of M″ is shown in Fig 6.34. It is obvious from the figure that the maximum peak shifts to the higher frequency side with increasing temperature. The asymmetric nature of the peaks indicates non-Debye relaxation.
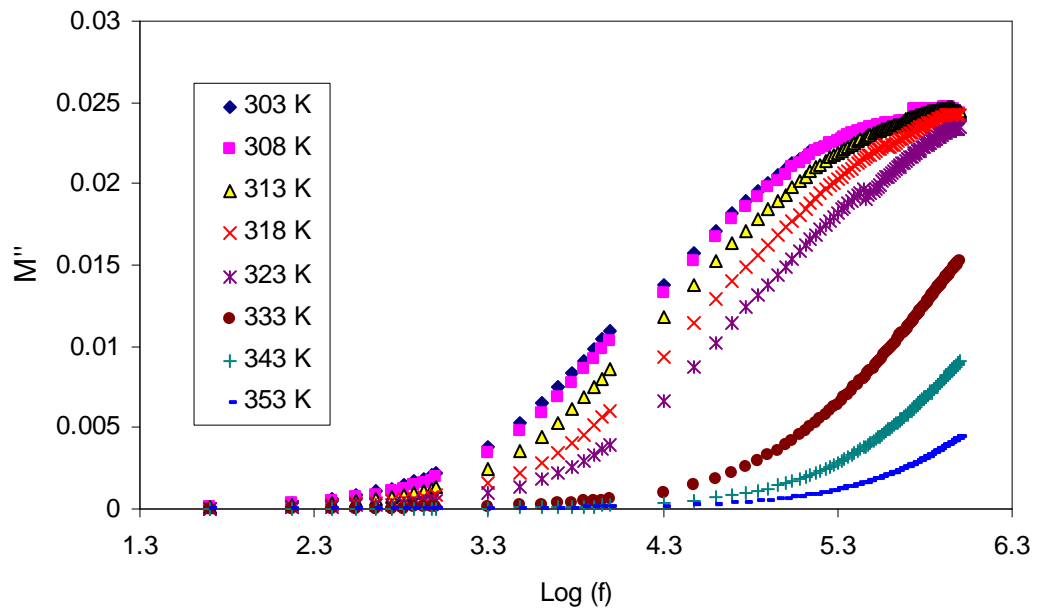
Figure 6.34 Frequency dependence of *M″* at different temperature for CSNB2 sample.

Figure 6.35 shows the Argand plots at different temperatures. It is obvious that the Argand plots exhibit incomplete semicircular arc. This satisfies that the relaxation processes is non-Debye type (single relaxation time) in the studied system (CSNB2). The non-Debye behavior is due to the contribution of different polarization mechanisms (ionic, dipolar, interfacial and electronic) in polymer electrolytes and thus a distribution of relaxation times. Moreover it can be seen that with increasing temperature *M″-M′* plot more deviate from the semicircular arc. This can be ascribed to the increase in conductivity and the disappearance of the high frequency semicircle. This can also be deduced from the M′ and M″ equations ($M' = \omega C_o Z_i$, $M'' = \omega C_o Z_r$). Thus the results of the second nano-composite electrolyte (1-x)(0.9CS:0.1NaTf)-xAl$_2$O$_3$ ($0.02 \leq x \leq 0.1$) system fortunately support the previous results of the first nano-composite solid electrolyte system, i. e., viscoelastic relaxation is governs the ionic conductivity.
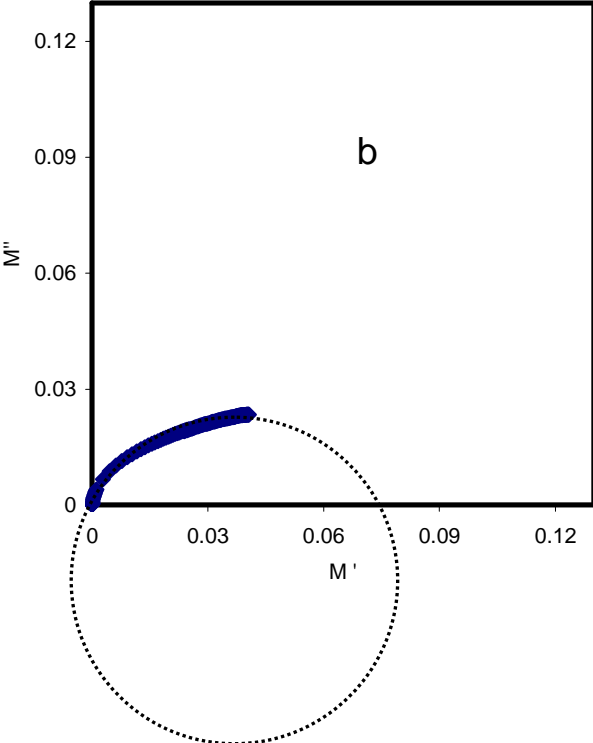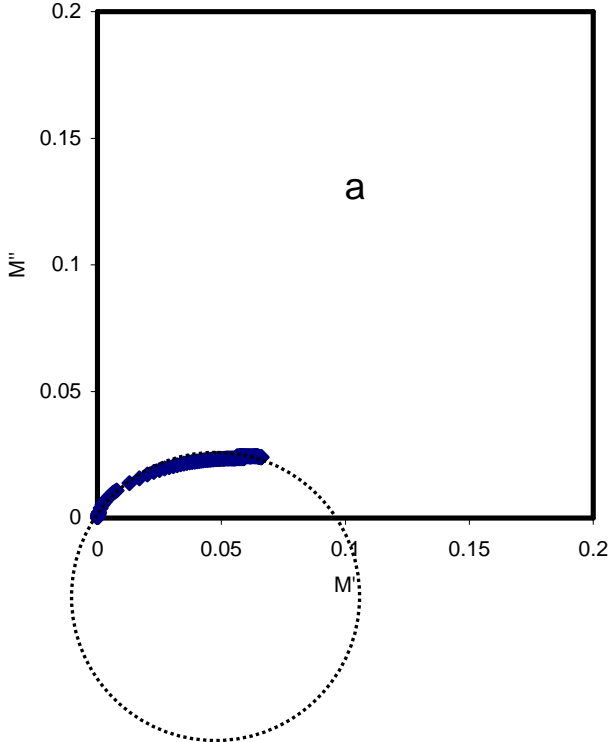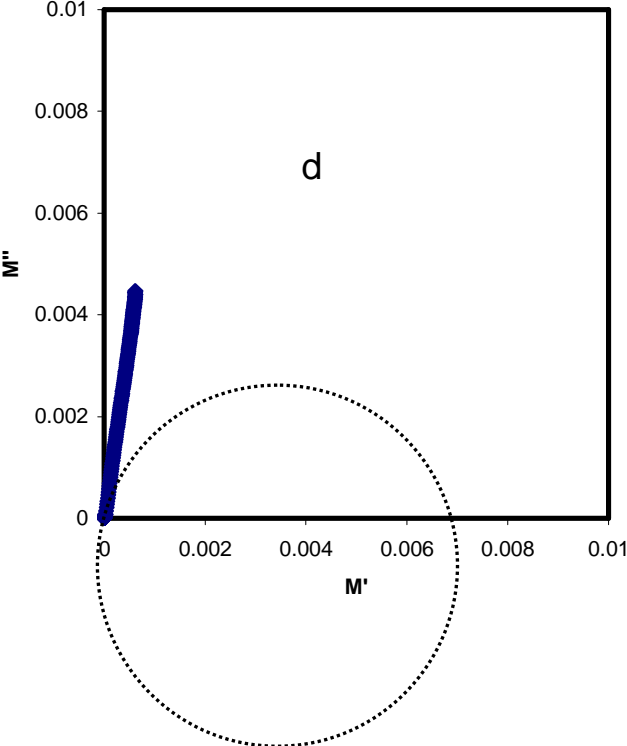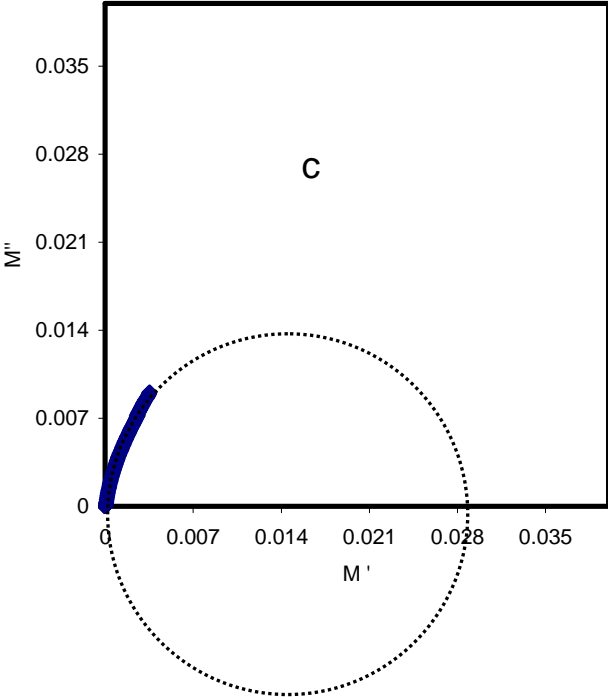
Figure 6.35 Argand plots for NCPE (CSNB2) at (a) 303 K, (b) 323 K, (c) 343 K and (d) 353 K.

6.3.4 Correlation between impedance and AC conductivity (σ_{ac}) in NCPEs (CSNB2).

Figure 6.36 (a-f) shows the Nyquist plot for NCPE based on CSNB2. At low temperatures from 303 to 333 K two regions are demonstrated. The low frequency region is due to the charge diffusion and accumulation at the electrode/ electrolyte interface (EP effect) which produces an electrical double layer capacitance. However the high frequency region (high frequency semi-circle), i. e., the bulk property of the material represents the charge transfer process in the bulk of the material [Hema et al., 2009]. It has been found that with increase in temperature; the semi-circle disappears suggesting that only the resistive component of the polymer prevails.
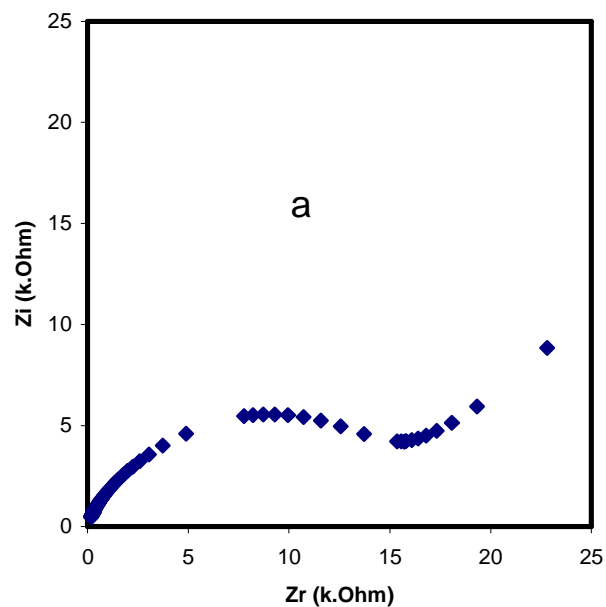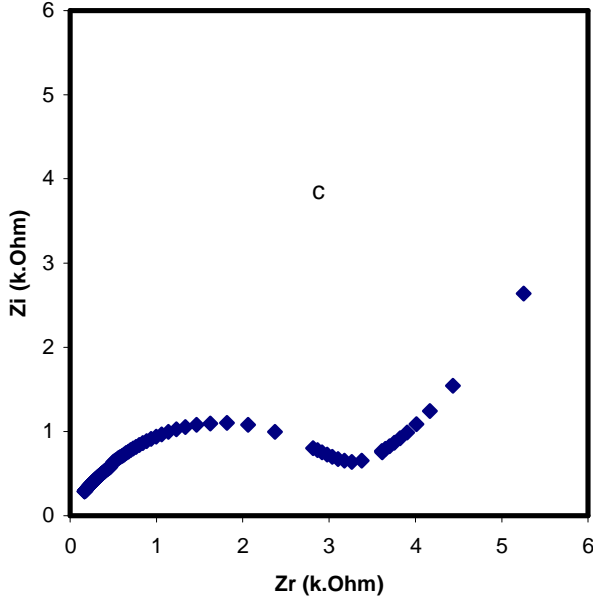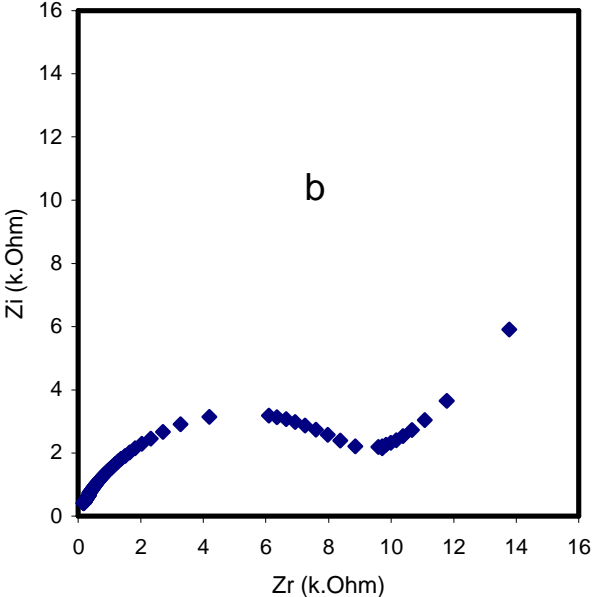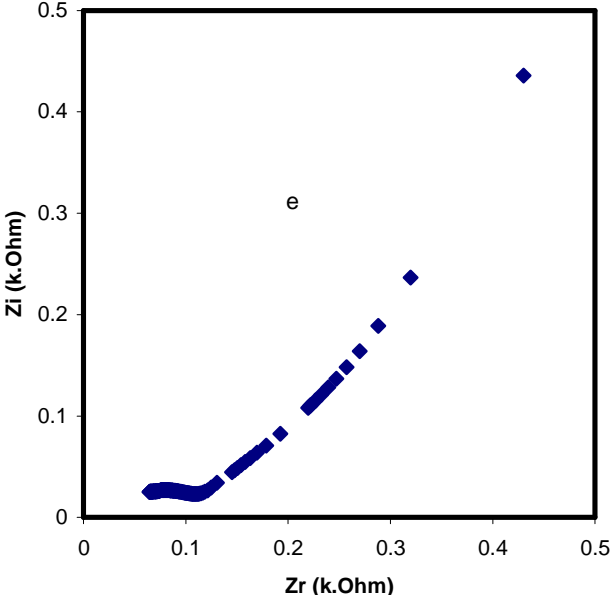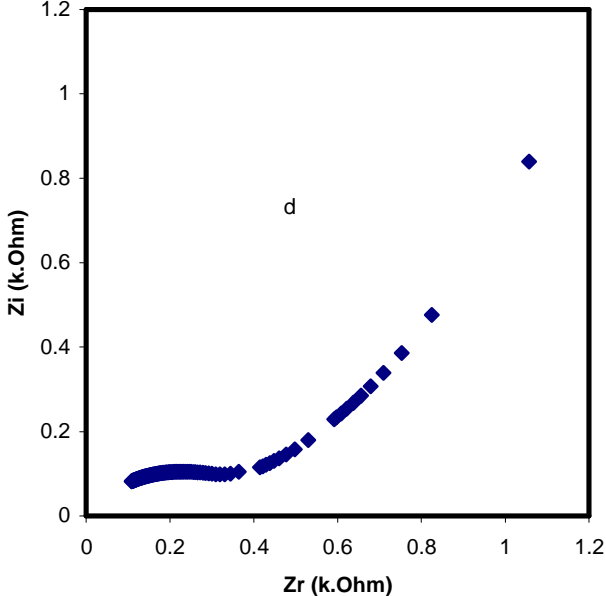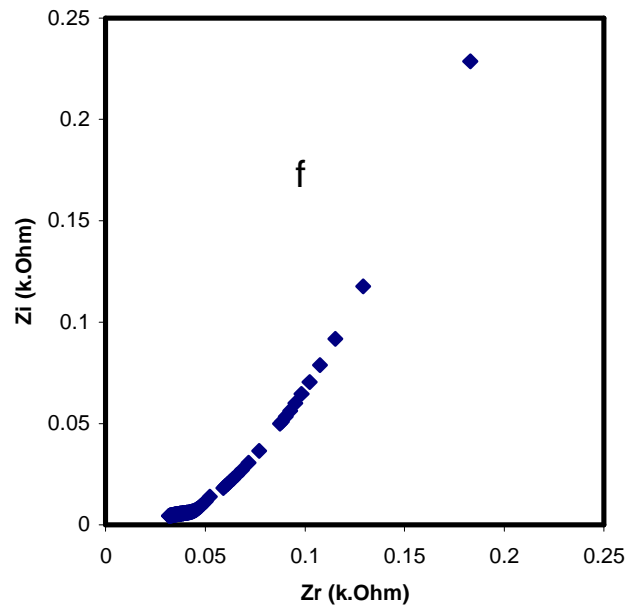
Figure 6.36 Impedance plots for NCPE (CSNB2) system at (a) 303 K, (b) 313 K, (c) 323 K, (d) 333 K, (e) 343 K, and (f) 353 K.

Figure 6.37 represents the AC conductivity spectra for CSNB2 sample at selected temperatures. The AC conductivity plot consists of three regions at low temperatures in the measured frequency range. The low frequency region due to the EP effect is followed by a plateau due to DC conductivity and the high frequency region which is important part of our study is due to bulk AC conductivity. It can be observed that the low frequency region (EP) becomes prominent and shifts to high frequency part as the temperature increases. The direct correlation between impedance plots and AC conductivity spectra reveals that when the high frequency semicircle (bulk) disappears, the high frequency AC conductivity dispersion also diminishes. These results specify that the AC conductivity dispersion is a bulk property of the material and is important to characterize the type of ion conduction in the bulk of the material via the calculation of the AC conductivity frequency exponent, s.
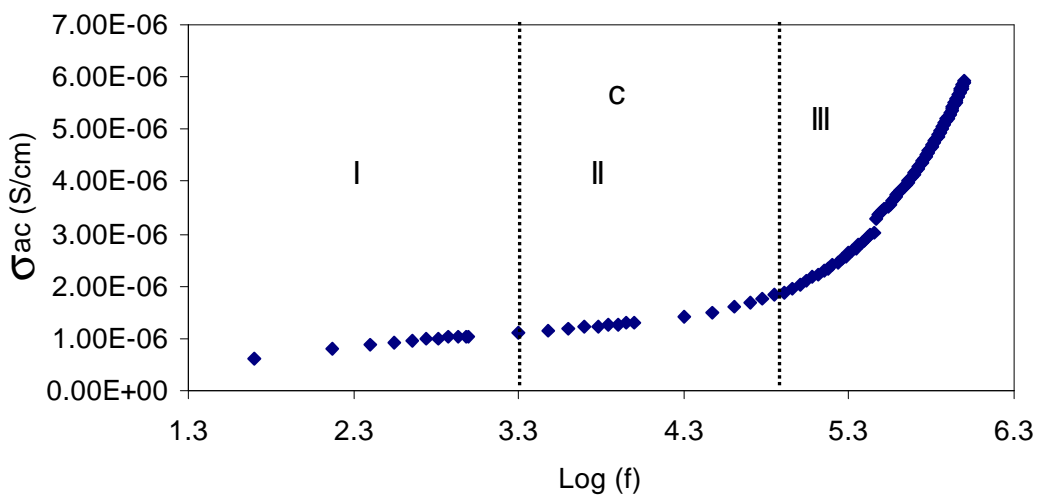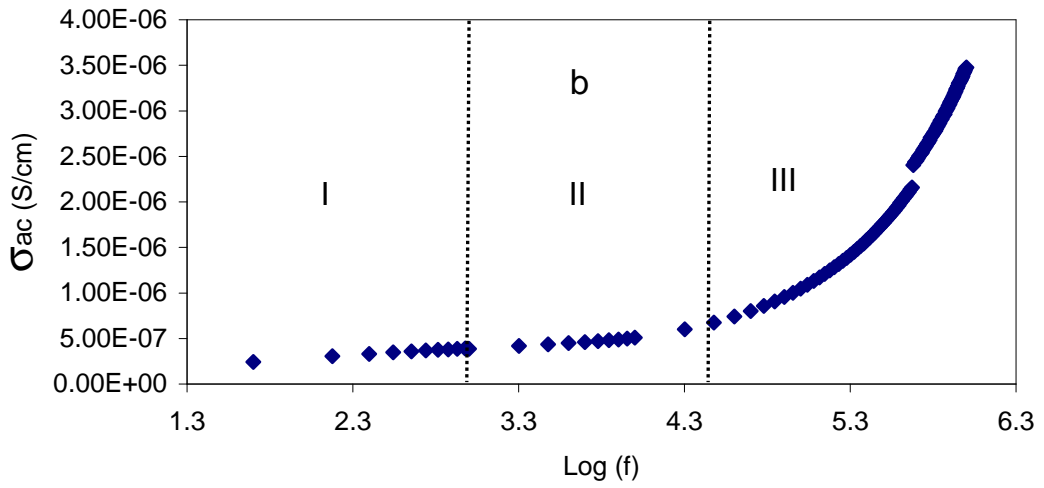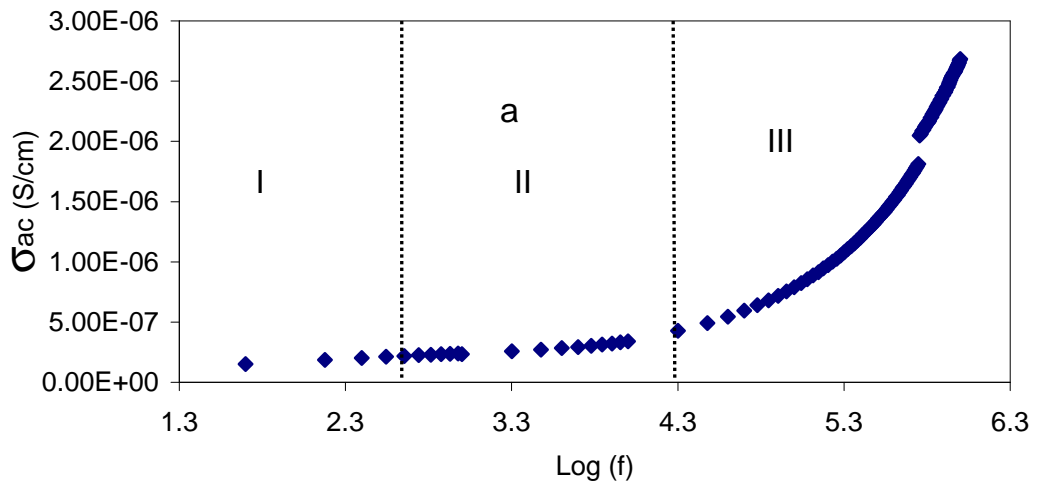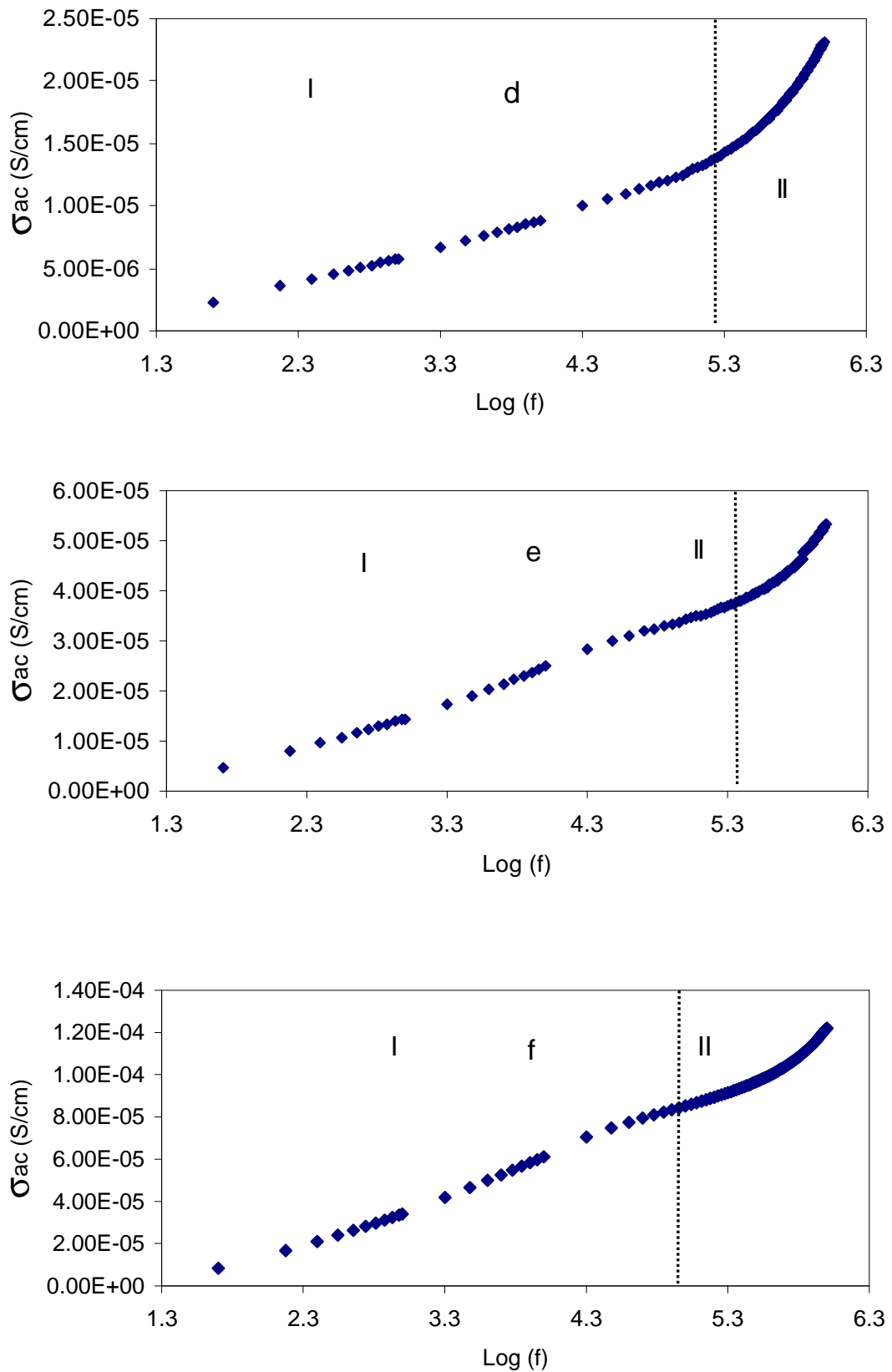
Figure 6.37 AC conductivity spectra for NCPE (CSNB2) system at (a) 303 K, (b) 313 K, (c) 323 K, (d) 333 K, (e) 343 K, and (f) 353 K.

Figure 6.38 shows the temperature dependence of the frequency exponent (s) for CSNB2 system. It is obvious that the s value decreases with increase in temperature. According to the correlated barrier hopping (CBH) model [Migahed et al., 2004], the frequency exponent s is found to decrease with increasing temperature to a minimum value. Thus the CBH model is the best model for this NCPE (CSNB2) system.
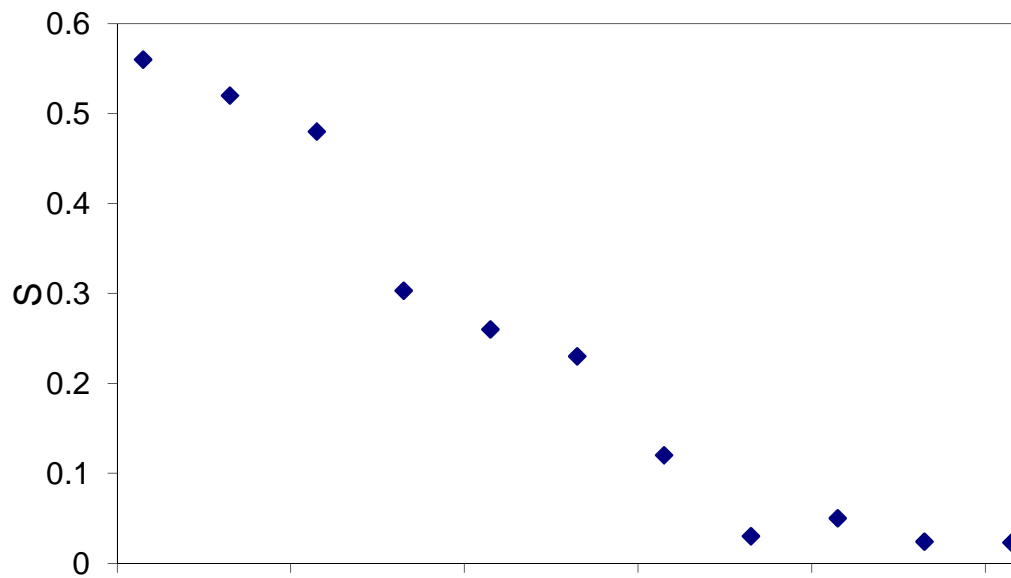
Figure 6.38 Temperature dependence of frequency exponent (s) for CSNB2 system.

6.4 Electrical/Dielectric properties of NCPEs based on (1-x)(0.9CS:0.1LiTf)-xAl$_2$O$_3$ (0.02 ≤ x ≤ 0.1)

6.4.1 DC conductivity and Dielectric analysis of NCPE based on (1-x)(0.9CS:0.1LiTf)-xAl$_2$O$_3$ (0.02 ≤ x ≤ 0.1)

Figure 6.39 shows the variation of DC conductivity for CS:LiTf (CSC6) sample with various concentrations of alumina nanoparticle. It is obvious that at low filler

concentrations (2 to 4 wt.%) the DC conductivity increased. However, at high filler concentrations (6 to 10 wt.%) the conductivity decreased. The high value of DC conductivity for $(1-x)(0.9CS:0.1LiTf)-xAl_2O_3$ $(0.02 \leq x \leq 0.1)$ nano-composites with respect to CS:LiTf (CSC6) solid polymer electrolyte again can be attributable to the effect of alumina nanoparticles. According to Stephan et al., (2006) the Lewis acid–base interaction centers reacts with the electrolytic species, thus lowering the ionic coupling and promotes the salt dissociation via a sort of ''ion–filler complex'' formation.
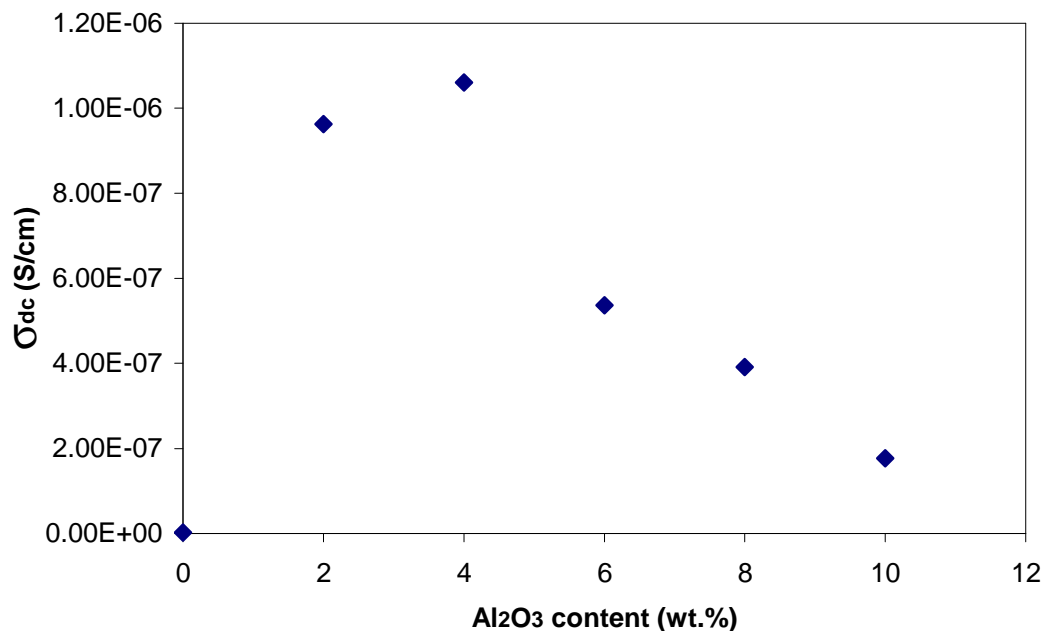
Figure 6.39 The ionic conductivity of chitosan:LiTf (CSC6) with various concentration of Al$_2$O$_3$.

Figure 6.40 shows the Arrhenius plot of nano-composite polymer electrolytes based on $(1-x)(0.9CS:0.1NaTf)-xAl_2O_3(0.02 \leq x \leq 10)$. It is interesting to note that in the third nano-composite electrolyte system the DC conductivity for all compositions again dropped at a particular temperature which is about 120 °C. Jiansirisomboon and Watcharapasorn (2008), observed and reported the phase transition of nano-composite

$BaTiO_3:Al_2O_3$ in the temperature range from 118 to 125°C using dielectric spectroscopy. The drop in DC conductivity in $(1-x)(0.9CS:0.1AgTf)-xAl_2O_3$ ($0.02 \leq x \leq 0.1$), $(1-x)(0.9CS:0.1NaTf)-xAl_2O_3$ ($0.02 \leq x \leq 0.1$) and $(1-x)(0.9CS:0.1LiTf)-xAl_2O_3$ ($0.02 \leq x \leq 0.1$) nanocomposite systems can thus be ascribed to the phase transition (Curie temperature) of Al_2O_3 nanoparticles. At Curie temperature the ferroelectric filler becomes a paraelectric and thus lose their spontaneous polarization. Consequently, drop in DC conductivity. It can be seen that the $(1-x)(0.9CS:0.1LiTf)-xAl_2O_3$ ($0.02 \leq x \leq 0.1$) nano-composite system shows similar behavior of DC conductivity with temperature which is non-Arrhenius at high temperatures. Similar behavior was reported for $PEO:LiTf:Al_2O_3$ and $PEO:LiTf:MgO$ composite polymer electrolytes [Dissanayakea et al., 2003, Kumar et al., 2002]. It is interesting to note that at higher temperatures the conductivity of all the compositions is close to each other. Similar behavior were observed for $PEO:LiTf:xAl_2O_3$ [Pitawala et al., 2007, Dissanayakea et al., 2003]. The calculated activation energy for the low temperature (303-333 K) region is 0.784 eV.
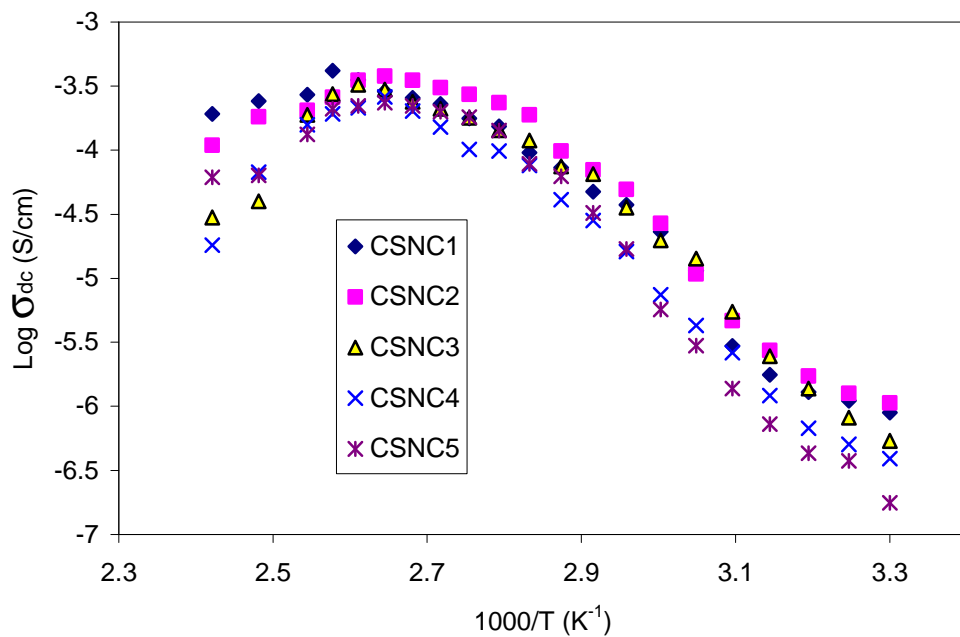
Figure 6.40 Temperature dependence of ionic conductivity of $(1-x)(0.9CS:0.1LiTf)-xAl_2O_3$ ($0.02 \leq x \leq 0.1$) NCPEs.

Figure 6.41 shows the frequency dependence of dielectric constant for different alumina concentrations. The high value of dielectric constant at low frequency can be ascribed to electrode polarization effect. These high dielectric constants at low frequencies are responsible for the suppression of high frequency dielectric constant for all the compositions to a single curve.
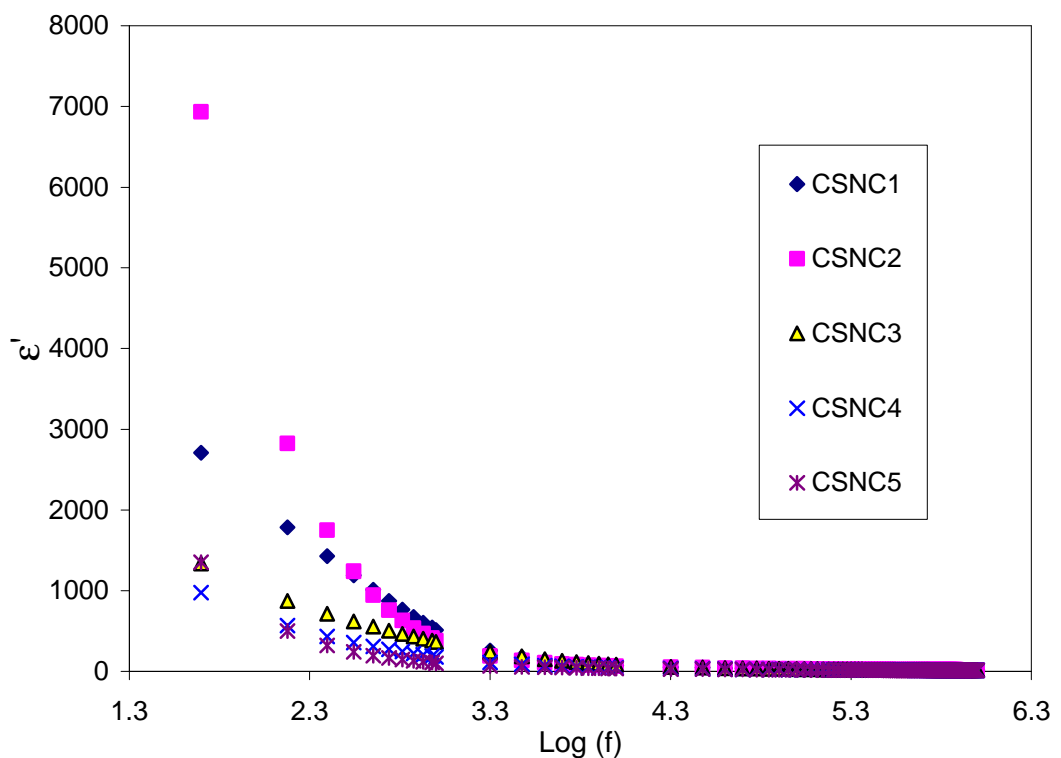
Figure 6.41 Composition dependence of dielectric constant for (1-x)(0.9CS:0.1LiTf)-xAl$_2$O$_3$ (0.02 ≤ x ≤ 0.1) NCPEs.

Figure 6.42 shows that the high frequency dielectric constant is also greatly influenced by the filler concentration. The high frequency dielectric constant is important because it represents the intrinsic property of the material and is directly related to DC conductivity.
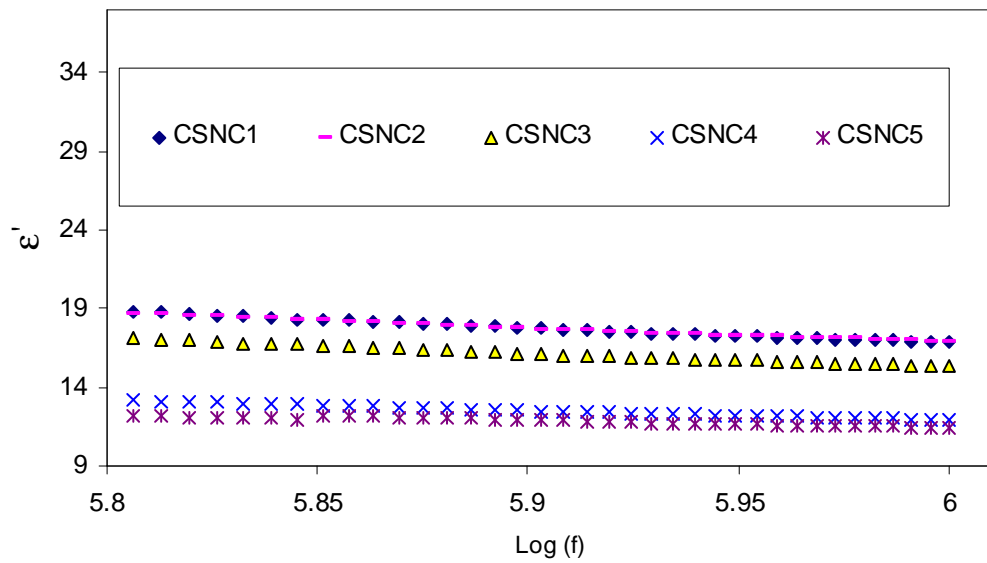
Figure 6.42 Composition dependence of bulk dielectric constant for CS:LiTf(90:10):xAl$_2$O$_3$ (2≤ x ≤ 0.1) NCPEs.

Figure 6.43 depicts the concentration dependence of bulk dielectric constant and DC conductivity.
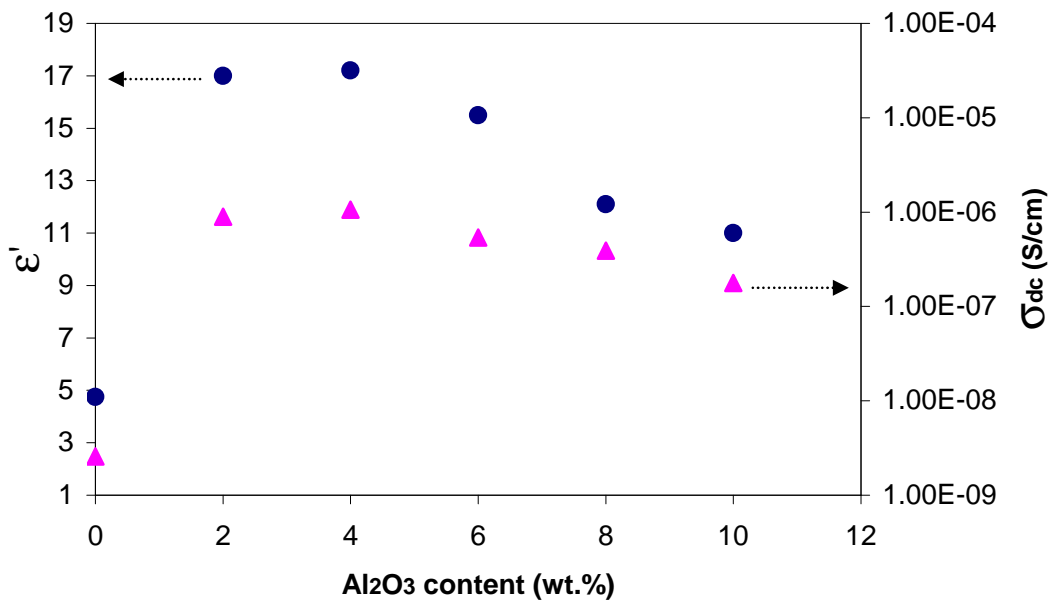
Figure 6.43 Dependence of Bulk dielectric constant and DC conductivity of chitosan:LiTf (CSC6) on Al$_2$O$_3$ concentration.

It is interesting to note that the behavior of bulk dielectric constant and DC conductivity (Fig. 6.43) with filler concentration is almost the same. Thus the DC conductivity-dielectric study in the third nano-composite system ((1-x)(0.9CS:0.1LiTf)-xAl$_2$O$_3$(0.02 ≤ x ≤ 0.1)) strongly supports the other two nano-composite systems ((1-x)(0.9CS:0.1AgTf)-xAl$_2$O$_3$(0.02 ≤ x ≤ 0.1), (1-x)(0.9CS:0.1NaTf)-xAl$_2$O$_3$(0.02 ≤ x ≤ 0.1)) results. These results suggest the strong correlation between DC conductivity and dielectric constant.

Figure 6.44 shows the dielectric constant as a function of frequency at different temperatures. The dielectric constant study at different temperatures may give further information between DC conductivity and dielectric constant. It can be seen that with increasing temperature the dielectric constant is also increased. The large value of dielectric constant (ε') at low frequency is attributable to EP effect which suppressed the bulk dielectric constant to a single curve.
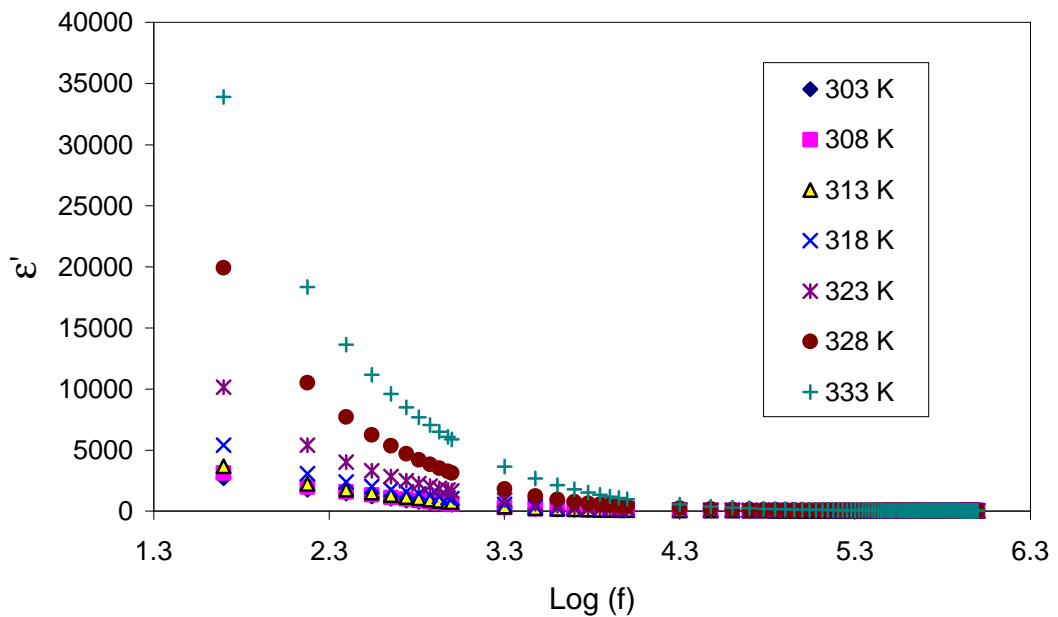
Figure 6.44 Frequency dependence of dielectric constant at different temperatures for CSNC2 system.

Figure 6.45 shows the frequency dependence of the bulk dielectric constant at different temperatures. It is interesting to note that the bulk dielectric constant is also temperature dependent. This indicates that bulk DC conductivity and bulk dielectric constant are strongly correlated.
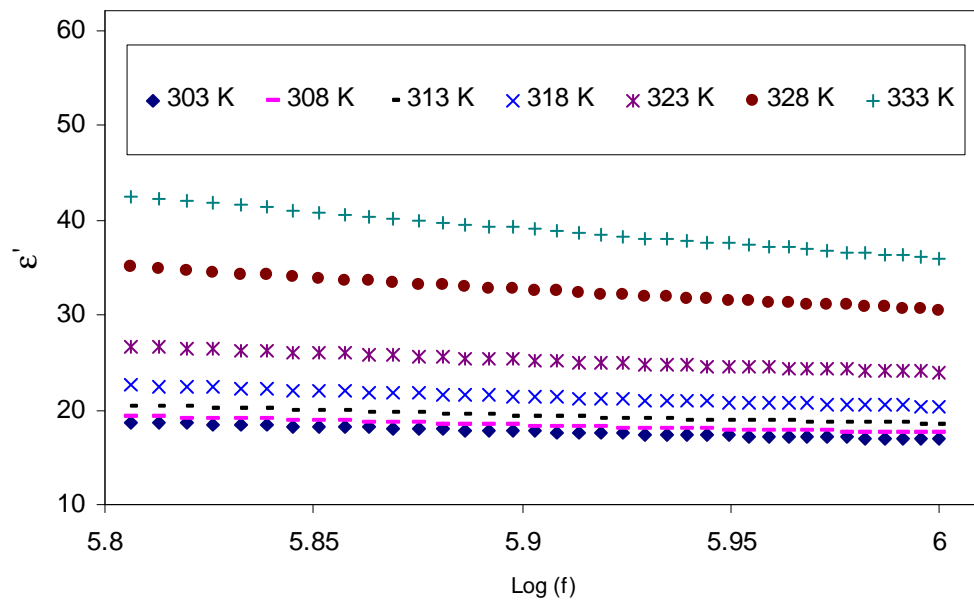
Figure 6.45 Frequency dependence of bulk dielectric constant at different temperatures for CSNC2 system.

Figure 6.46 shows the smooth curve between DC conductivity and bulk dielectric constant at selected temperatures. It is obvious from the plot that the bulk DC conductivity is smoothly increased with increasing bulk dielectric constant at different temperatures. Thus the third nanocomposite $((1-x)(0.9CS:0.1LiTf)-xAl_2O_3$ $(0.02 \leq x \leq 0.1))$ system show similar behavior between DC conductivity and bulk dielectric constant like the other two nanocomposite $((1-x)(0.9CS:0.1AgTf)-xAl_2O_3$ $(0.02 \leq x \leq 0.1)$ and $(1-x)(0.9CS:0.1NaTf)-xAl_2O_3$ $(0.02 \leq x \leq 0.1))$ systems at different

temperatures. The concentration dependence of bulk DC conductivity and bulk dielectric constant together with the smooth curve between DC conductivity and dielectric constants confirm the dependence of DC conductivity on dielectric constant in NCPEs based on chitosan. The increase in dielectric constant means an increase in carrier density and hence an increase in DC conductivity.
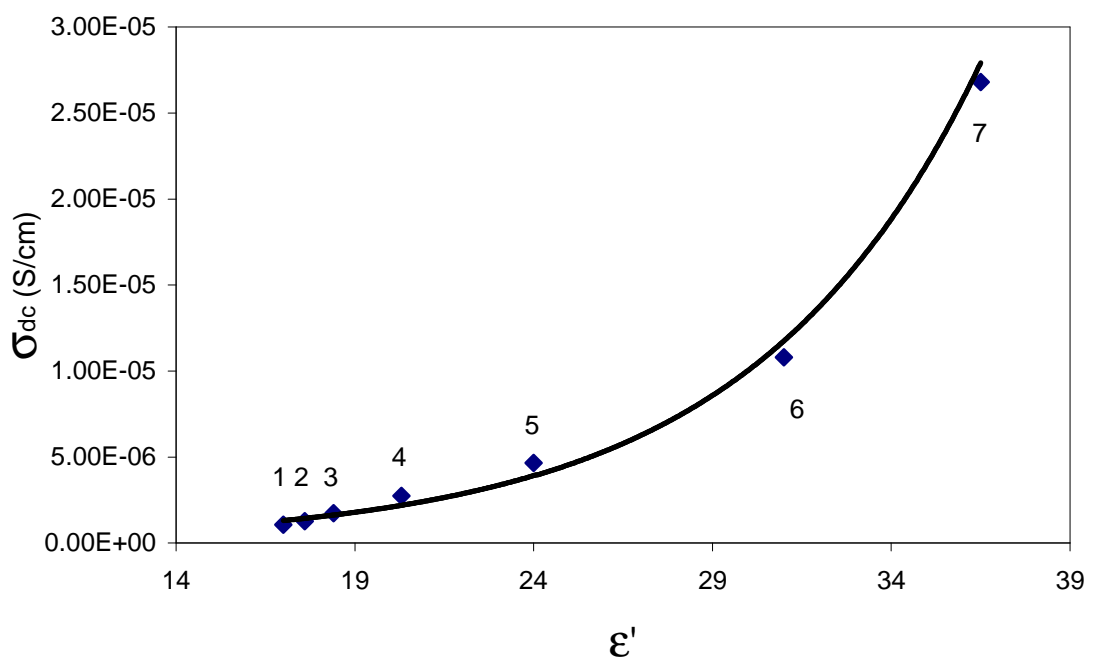
Figure 6.46 DC conductivity dependence on dielectric constant at, (1) 303, (2) 308, (3) 313, (4) 318, (5) 323, (6) 328 and (7) 333 K for CSNC2 system.

One point of DC conductivity can be selected in Fig. 6.46 as a reference to scale the DC conductivity and studying the compensated Arrhenius equation. Figure 6.47 shows the compensated Arrhenius behavior for CSNC2 sample. The behavior of compensated Arrhenius (Fig. 6.47) with temperature is similar to the normal Arrhenius (Fig. 6.40). The slope gives activation energy of 0.799 eV in the low temperature region which is almost the same compared to the calculated one from normal Arrhenius relation. This

activation energy was used to calculate the pre-exponential factor by dividing the

conductivity with the quantity $\exp(-E_a / K_b T)$.
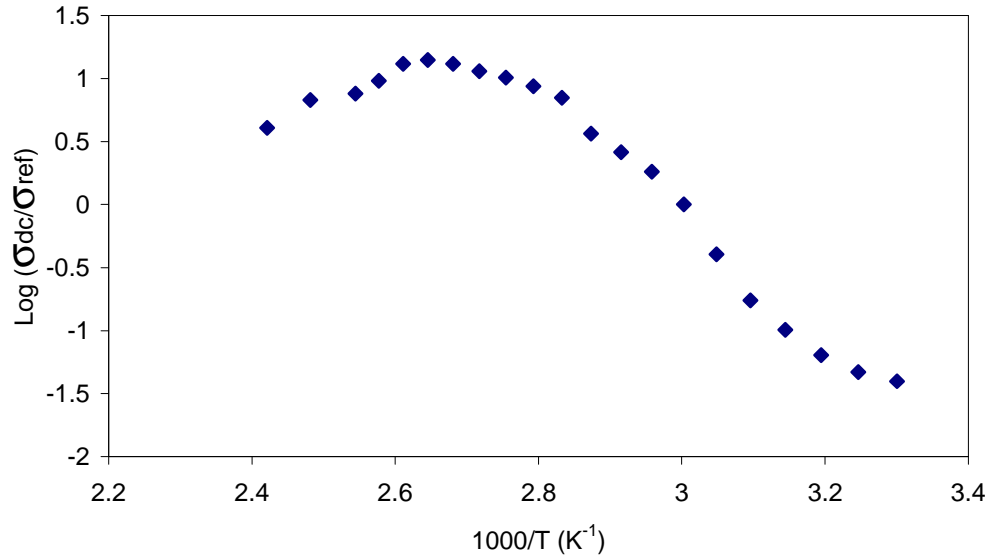
Figure 6.47 Compensated Arrhenius equation plotted against the reciprocal temperature for CSNC2 system.

The temperature and dielectric constant dependence of pre-exponential factor for

CSNC2 is shown in Figure 6.48.
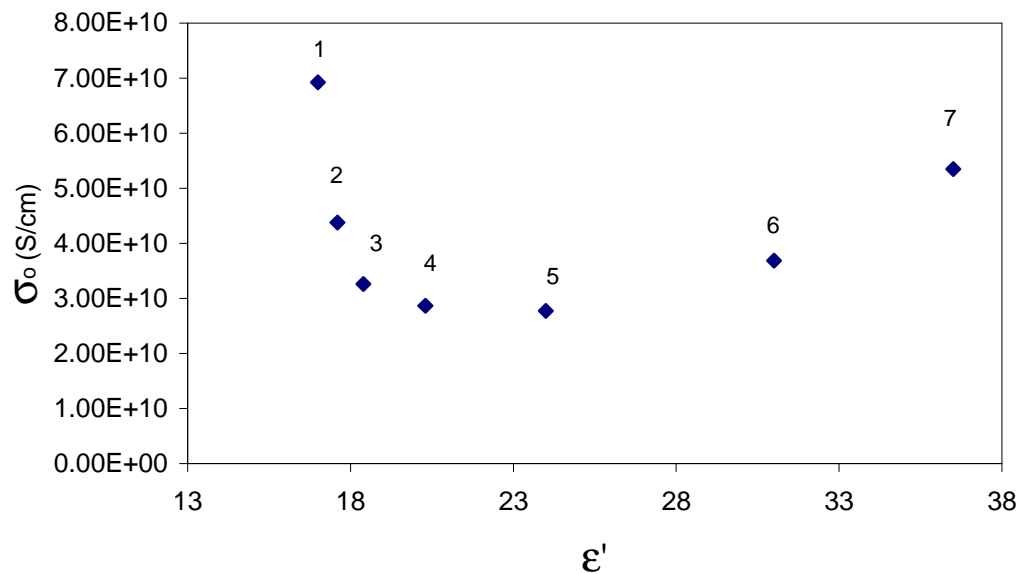
Figure 6.48 Temperature and dielectric constant dependent of pre-exponential factor (σ_o) at (1)303, (2) 308, (3) 313, (4) 318, (5) 323, (6) 328 and (7) 333 K for CSNC2 system.

The absence of smooth curve between the pre-exponential factor and dielectric constant (Fig. 6.48) indicated the non applicability of the compensated Arrhenius equation. Fortunately the third nano-composite solid polymer electrolyte $(1-x)(0.9CS:0.1LiTf)-xAl_2O_3$ $(0.02 \leq x \leq 0.1)$, reveal the constant behavior of pre-exponential factor.

Figure 6.49 shows the variation of dielectric loss with frequency at different temperatures for CSNC2 system. The high value of dielectric loss at low frequency is attributable to EP effect as a result of charge carrier motion and accumulation at the electrode/electrolyte interface. It can be seen that the dispersion of dielectric loss spectra shifts to the high frequency part with increasing temperature as a result of high charge carrier dissociation and accumulation.
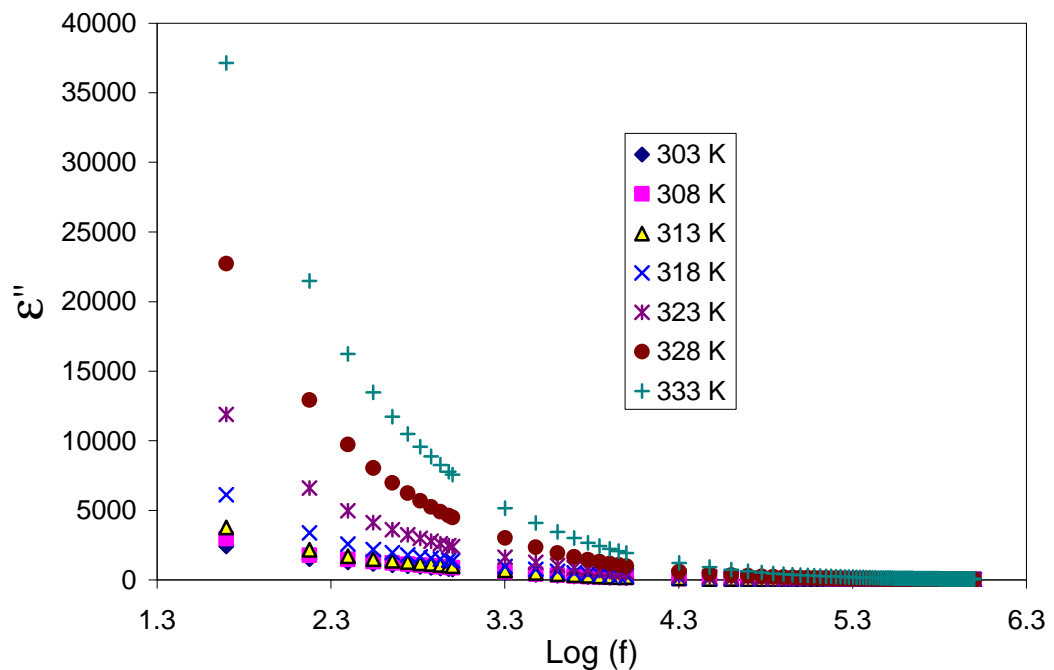
Figure 6.49 frequency dependence of dielectric loss at different temperatures for CSNC2 system.

6.4.2 Frequency dependence of tan δ for NCPE (CSNC2) system

Figure 6.50 shows the variation of dielectric loss tangent as a function of frequency at selected temperatures. It can be seen that the tan δ peak shifts to high frequency with increasing temperature. This indicates the decrease of relaxation time and the broadness of the peaks can be ascribed to non-Debye relaxation.
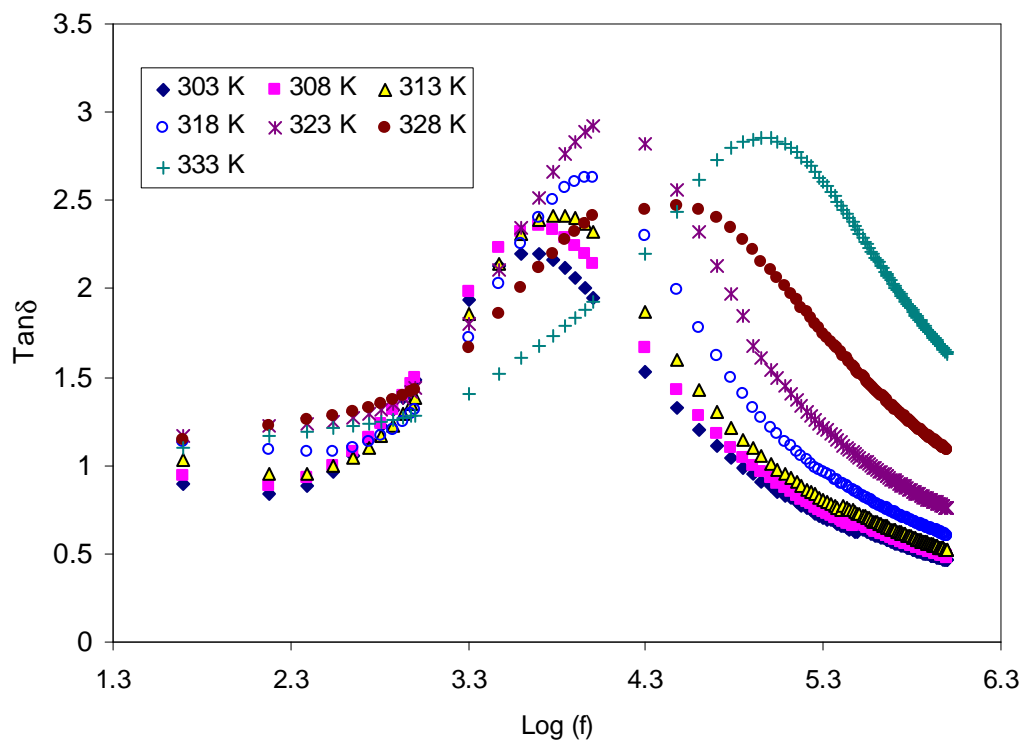
Figure 6.50 Frequency dependence of loss tangent (tanδ) at different temperatures for CSNC2 sample.

Figure 6.51 shows the temperature dependence of relaxation frequency. The rise in temperature causes the drop in relaxation time due to the increased of ionic conductivity. It can be seen that all the points lie on a straight line. The calculated activation energy is 0.754 eV.
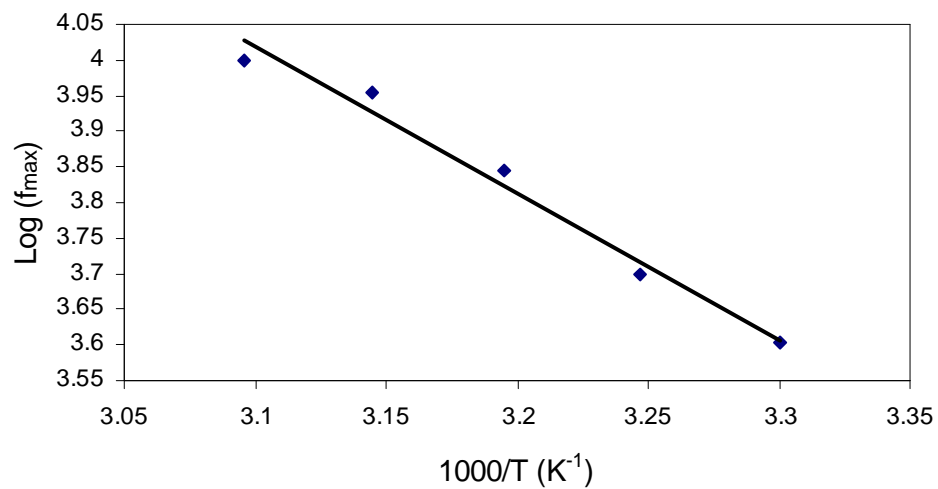
Figure 6.51 Temperature dependence of relaxation frequency for CSNC2 system.

6.4.3 Electric modulus analysis of CSNC2 system: Relaxation processes

Figure 6.52 depicts the frequency dependence of real part of electric modulus at different temperatures. The observed long tail at low frequencies is attributable to the large value of electrode polarization capacitance. The decrease in M' value at high temperature is due to the decrease of resistance of the sample and increase in electrode polarization.
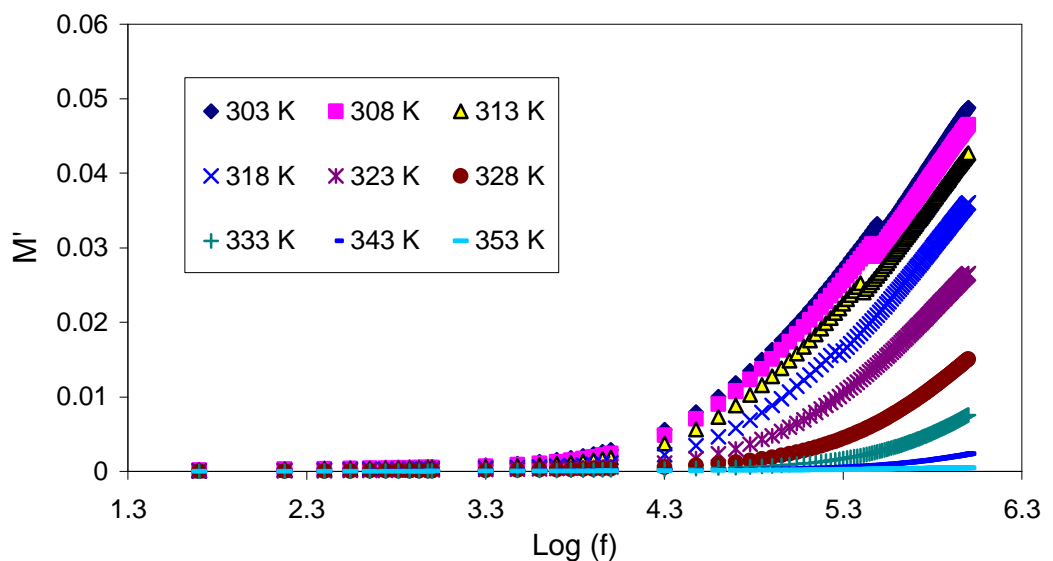
Figure 6.52 Frequency dependence of M' at different temperature for CSNC2 sample.

Figure 6.53 shows the variation of imaginary part of electric modulus with frequency at selected temperatures. At low temperatures peaks were observed. The peaks are asymmetric and broad which indicate the distribution of relaxation times. However at high temperatures the peaks disappeared possibly due to the frequency limitation.
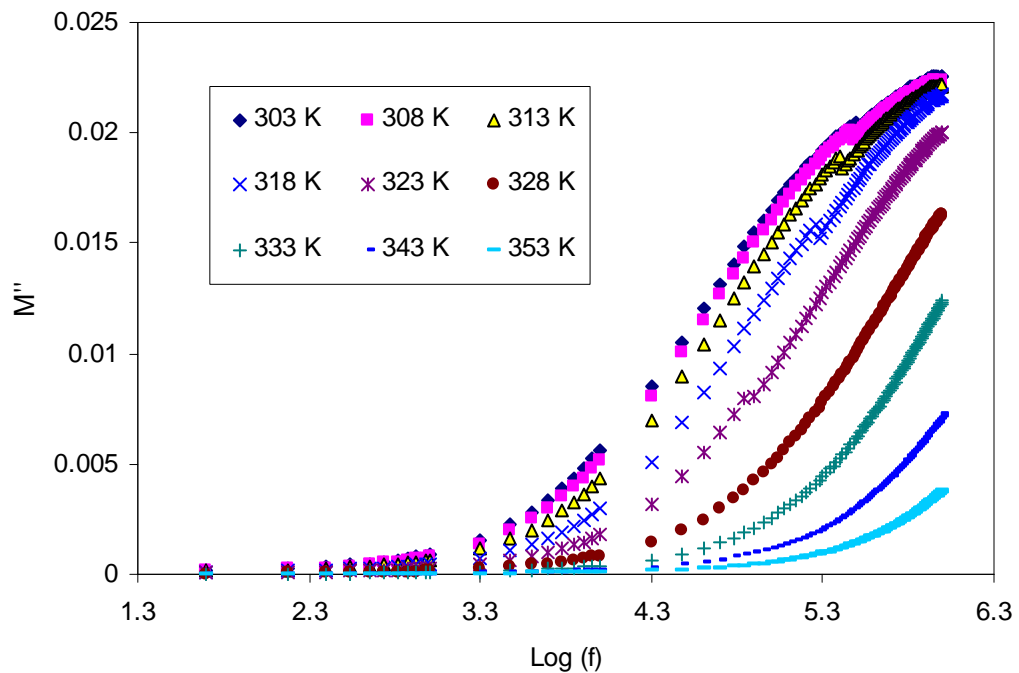
Figure 6.53 Frequency dependence of *M″* at different temperature for CSNC2 sample.

The Argand plots at different temperatures for the NCPE (CSNC2) are shown in Figure 6.54. It can be seen that the Argand plots exhibits incomplete semicircular arc. This indicates the non-Debye type relaxation process. The Debye model is developed to non interacting identical dipoles [Hill and Dissado, 1985]. Thus the non-Debye behavior is due to the fact that in real material there are more than one type of polarization mechanisms and a lot of interactions between ions and dipoles. These results in a

distribution of relaxation times. Moreover it can be seen that with increasing temperature M''-M' curve deviates more from the semicircular arc. This can be ascribed to the increase in conductivity. With increase in temperature the Z_i and Z_r values are decrease and thus the M" and M′ values ($M'' = \omega C_o Z_r$, $M' = \omega C_o Z_i$) are more deviate towards the origin.
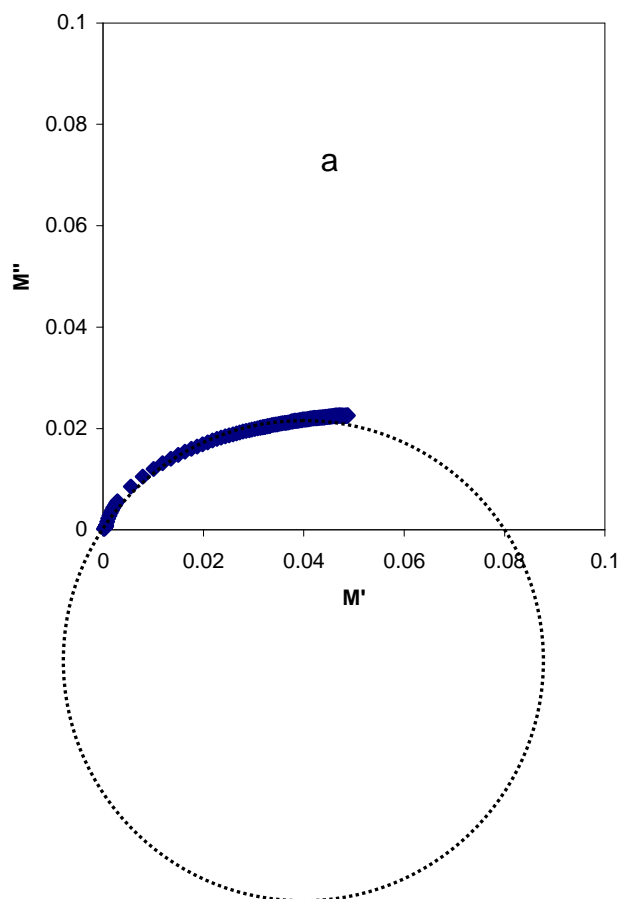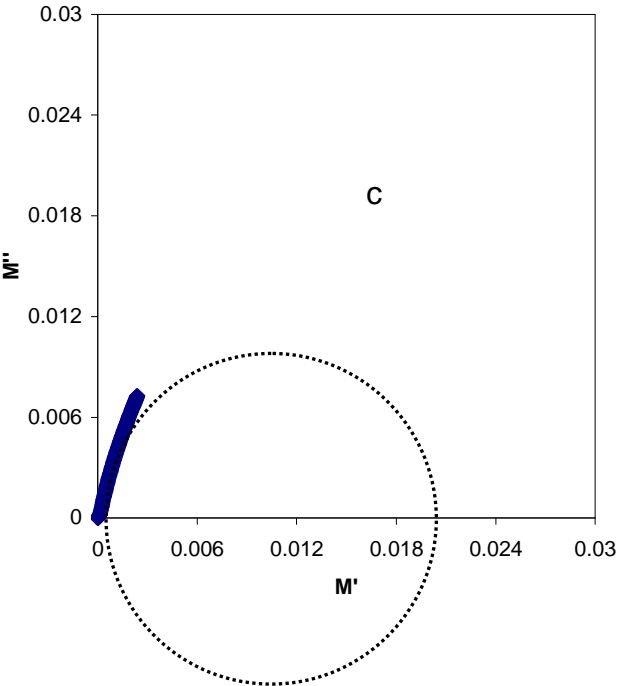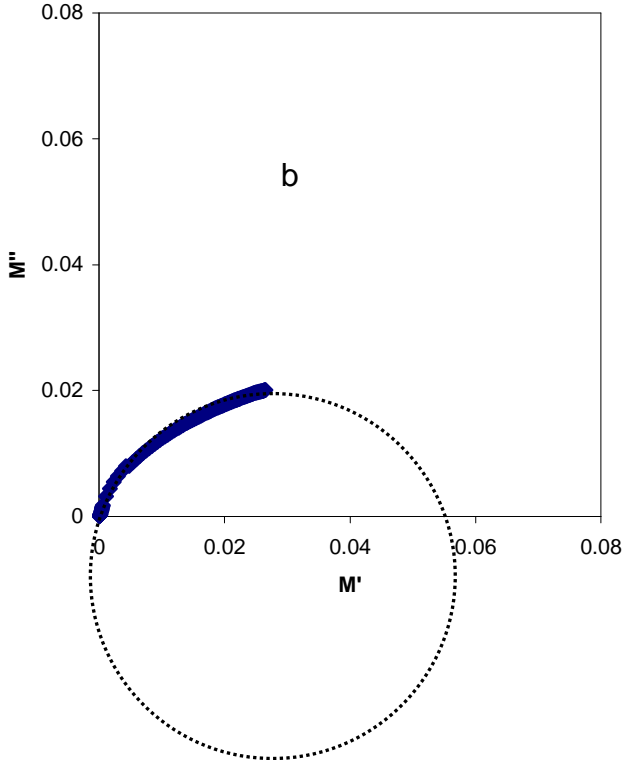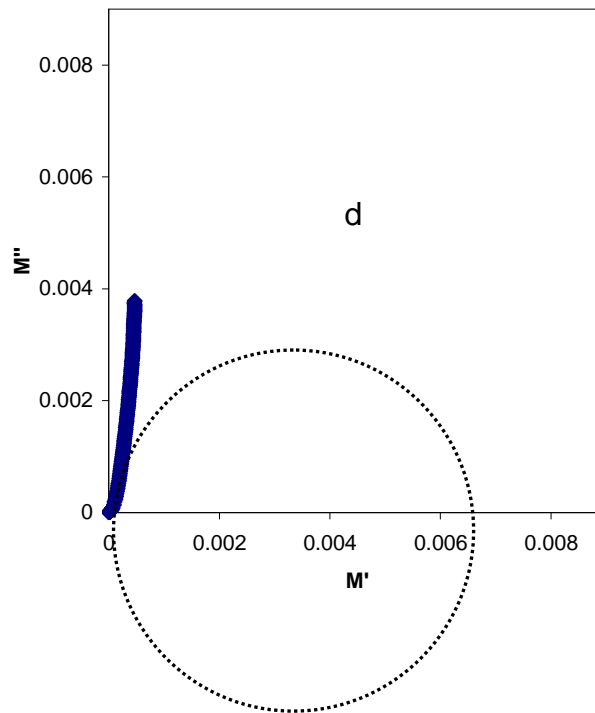
Figure 6.54 Argand plots for NCPE (CSNC2) at (a) 303 K, (b) 323 K, (c) 343 K and (d) 353 K.

6.4.4 Correlation between impedance and AC conductivity (σ_{ac}) in NCPE (CSNC2) system.

The typical Nyquist plot of impedance for NCPE (CSNC2) is presented in Fig. 6.55 (a-f). The impedance plot shows two distinct regions at low temperatures. The appearance of two semicircles in NCPEs was observed for the first time by Adebahr et al., (2006). They interpreted this phenomenon on the fact that the two semicircles indicate that there is a bulk and an interface contribution, alternatively two different phases. The bulk process due to ion conduction and the interface process due to the filler contribution. The disappearance of the high frequency semicircular portion in the complex impedance plot at high temperatures led to a conclusion that the current carriers are ions and this leads one to further conclude that the total conductivity is mainly the result of ion

conduction. At low frequency, the complex impedance plot must show a straight line parallel to the imaginary axis, but the double layer at the blocking electrodes causes the curvature.
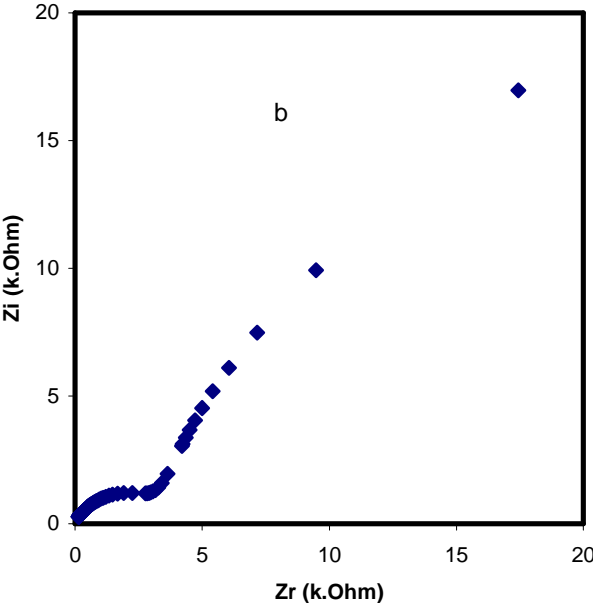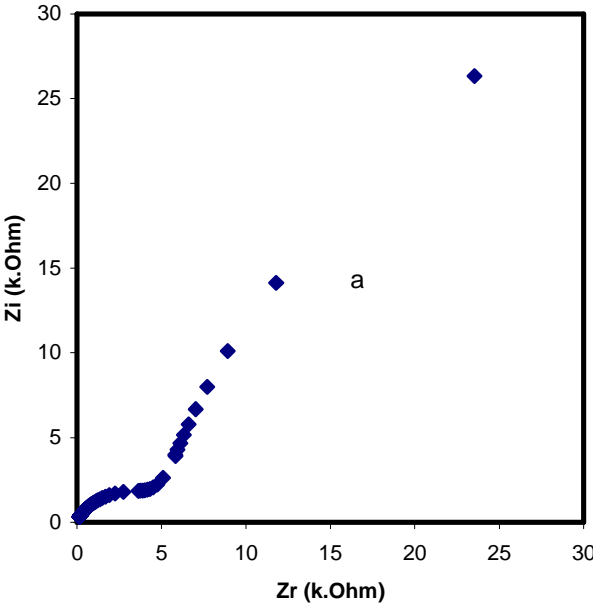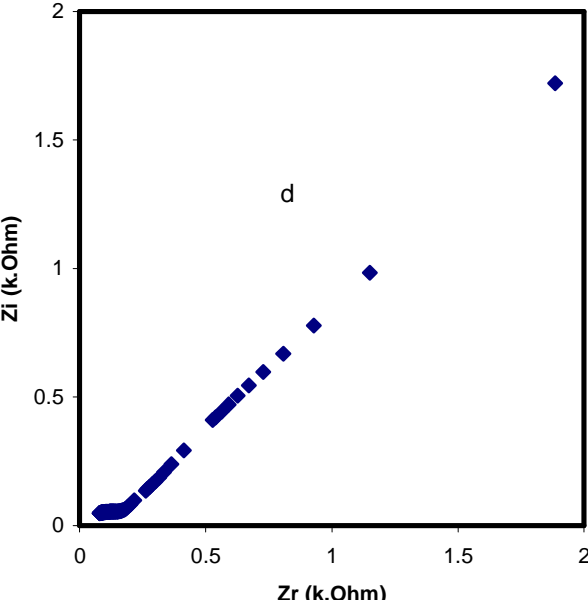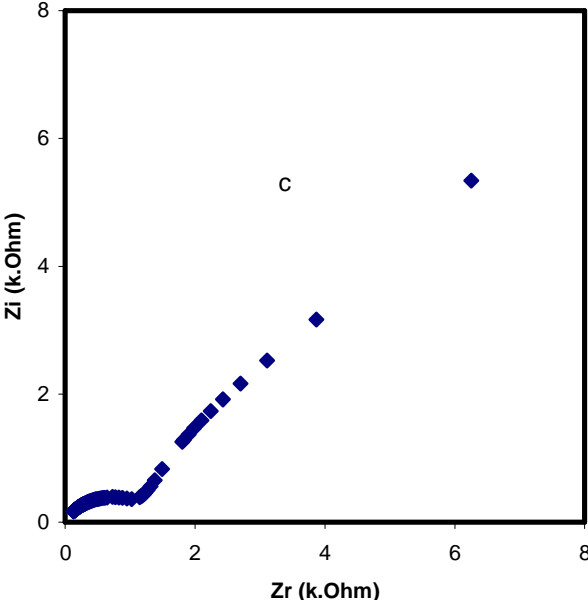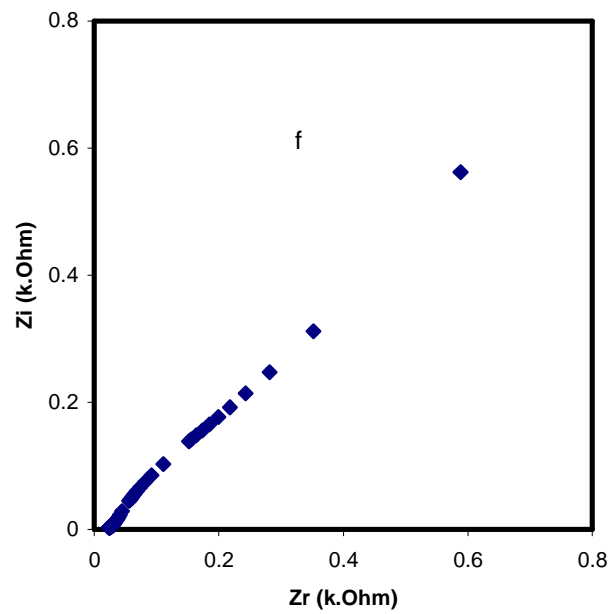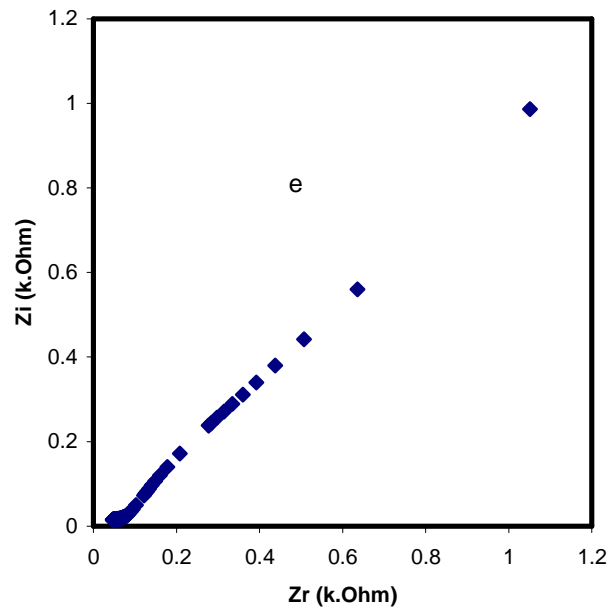
Figure 6.55 Impedance plots for NCPE (CSNC2) at (a) 303 K, (b) 313 K, (c) 323 K, (d) 333 K, (e) 343 K, and (f) 353 K.

Figure 6.56 (a-f) shows the frequency dependence of AC conductivity at selected temperatures for CSNC2 system. The figure shows three distinct regions at low temperatures and only two regions can be distinguished at high temperatures. It can be seen that with increasing temperature the electrode polarization (region I) is increased and the plateau region decreased and the dispersion region shifts to high frequency side. From the comparison of impedance plots and AC conductivity spectra we conclude that there is a strong correlation between high frequency semicircle (bulk) and AC conductivity dispersion region. These results specify that the AC conductivity dispersion is a bulk property of the material and is important to characterize the type of ion conduction in the bulk of the material via the calculation of the AC frequency exponent s.
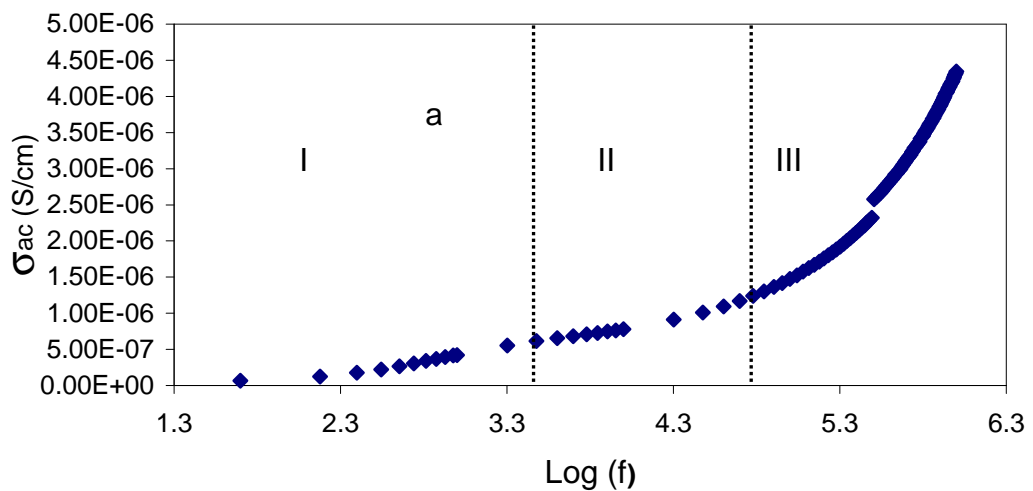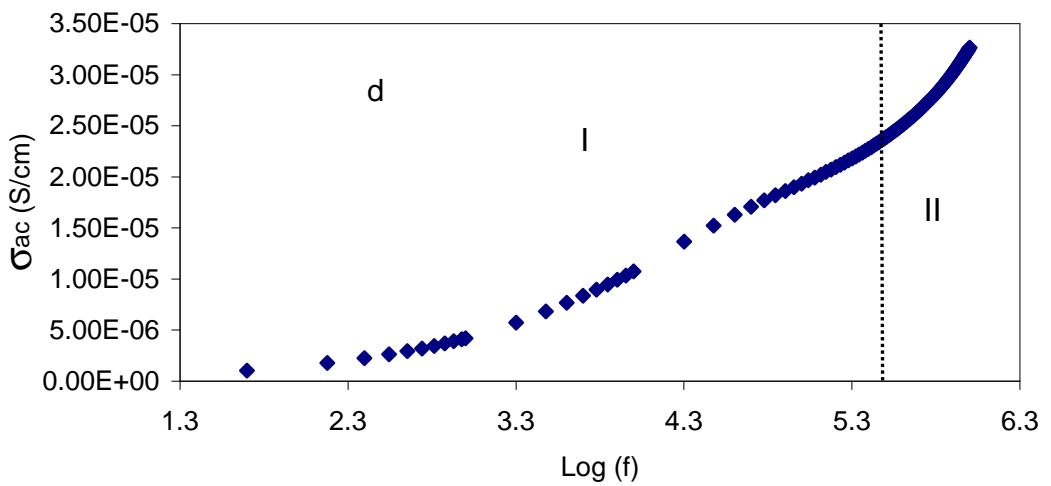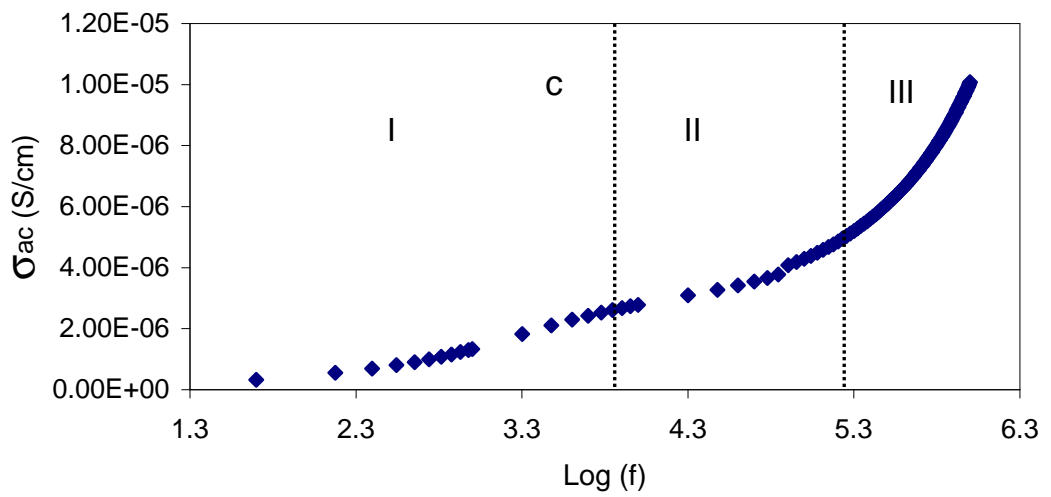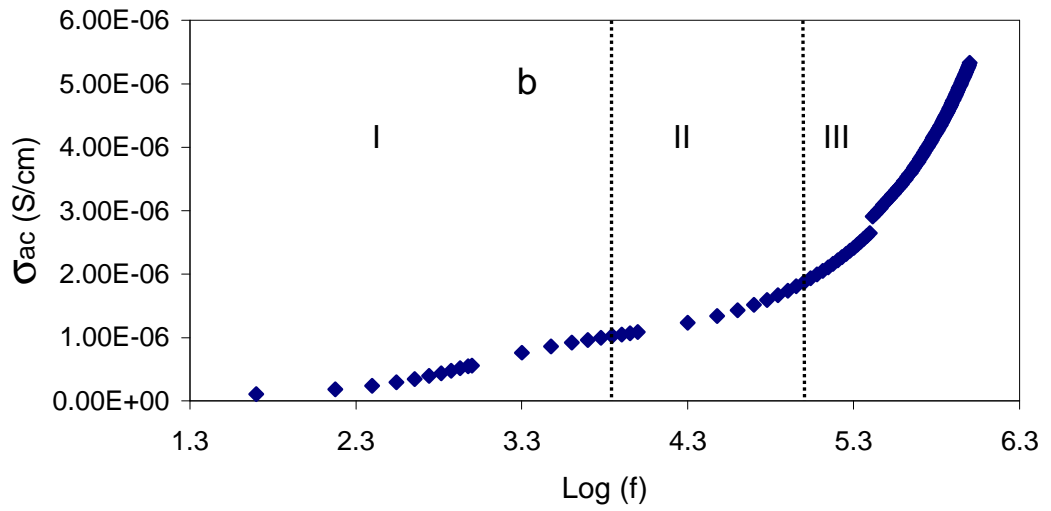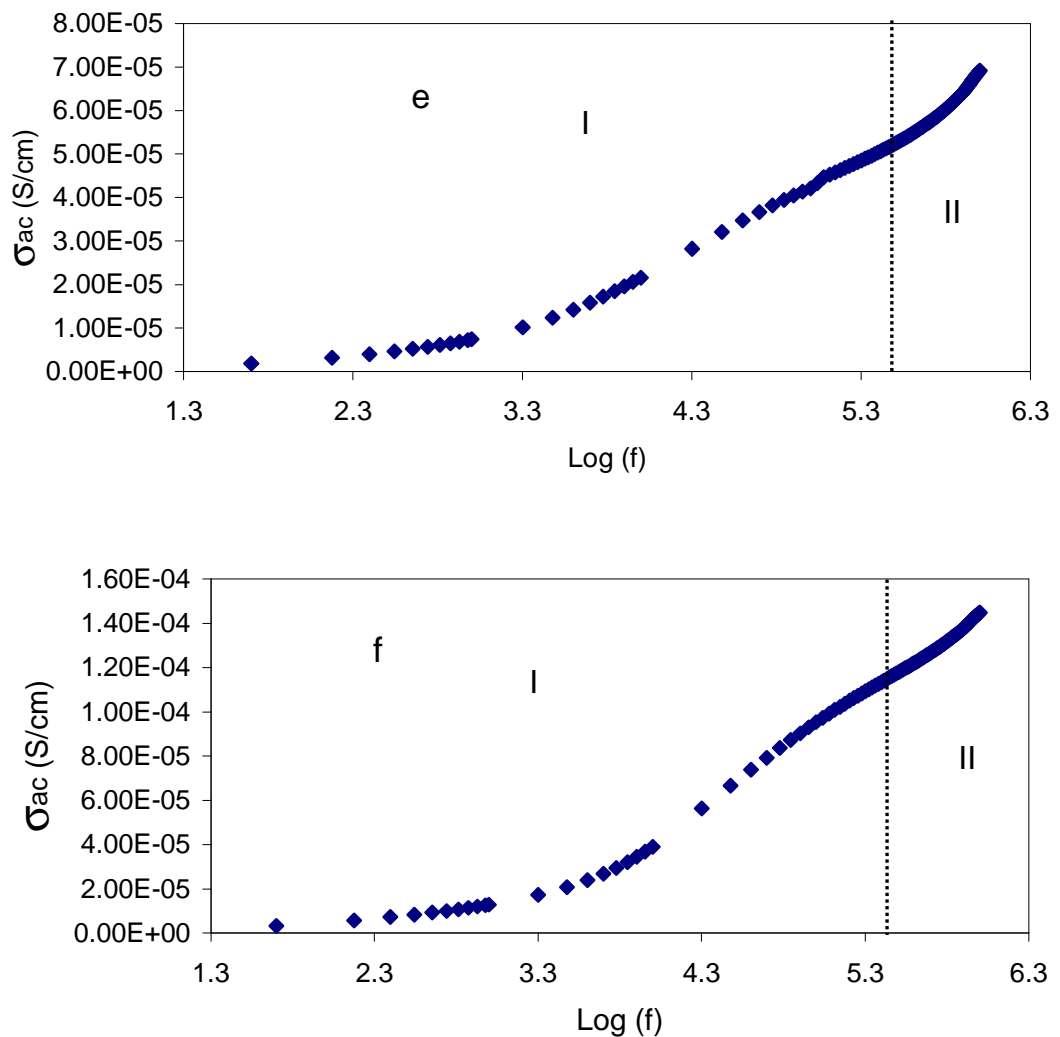
Figure 6.56 AC conductivity spectra for NCPE (CSNC2) at (a) 303 K, (b) 313 K, (c) 323 K, (d) 333 K, (e) 343 K, and (f) 353 K.

Figure 6.57 shows the temperature dependence of the frequency exponent (s) for CSNC2 system. It is obvious that the s value decreased with temperature increase to a minimum value. According to correlated barrier hopping (CBH) model [Migahed et al., 2004], the frequency exponent s is found to decrease with increasing temperature to a minimum value. Thus the CBH model again is the best model for this NCPE (CSNC2) system.
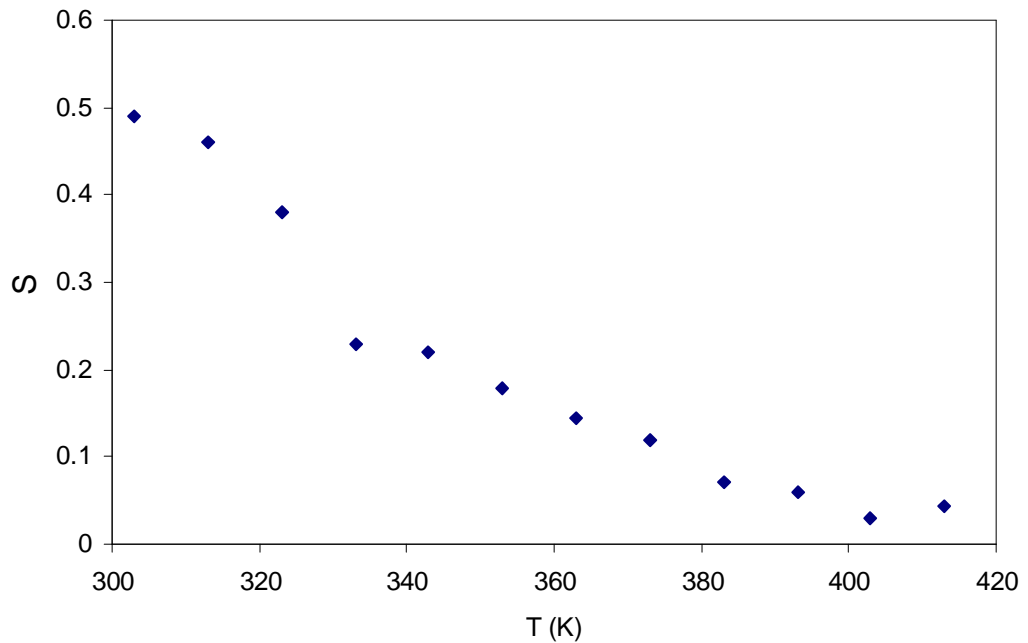
Figure 6.57 Temperature dependence of frequency exponent (s) for CSNC2 system.

6.5 Summary

The results of this chapter show the following interesting points:

(a) The role of alumina nanoparticles on DC conductivity and dielectric constant enhancement in $(1\text{-}x)(0.9CS:0.1AgTf)\text{-}xAl_2O_3(0.02 \leq x \leq 0.1)$, $(1\text{-}x)(0.9CS:0.1NaTf)\text{-}xAl_2O_3(0.02 \leq x \leq 0.1)$ and $(1\text{-}x)(0.9CS:0.1LiTf)\text{-}xAl_2O_3(0.02 \leq x \leq 0.1)$ nano-composite polymer electrolytes is demonstrated.

(b) The DC conductivity and dielectric constant results with Al_2O_3 concentration and at different temperatures indicate that the DC conductivity and dielectric constant are

correlated. The DC conductivity versus temperature reveals the VTF behavior at higher temperatures in these NCPEs.

(c) The DC conductivity of all the three NCPEs is dropped at a particular temperature which can be ascribed to the Curie temperature of the alumina nanoparticles.

(d) In these NCPEs the non applicability of compensated Arrhenius was demonstrated. The random distribution of pre-exponential factor with dielectric constant and temperature for these NCPEs indicates the applicability of Arrhenius equation.

(e) The relaxation processes in terms of Argand plots and tan δ plots of theses nano-composite solid polymer electrolytes supports the non-Debye relaxation type. The correlation between impedance plots and AC dispersion and the role of EP effect were demonstrated. The type of ion conduction for each system was specified from the temperature variation of the frequency exponent (s).